Origin of nitrate and sulfate sources in volcano-sedimentary aquifers of the East Africa Rift System: An example of the Ali-Sabieh groundwater (Republic of Djibouti)

Origin of nitrate and sulfate sources in volcano-sedimentary aquifers of the East Africa Rift System: An example of the Ali-Sabieh groundwater (Republic of Djibouti)

Mohamed Osman Awaleh[a*], Tiziano Boschetti[b], Abdillahi Elmi Adaneh[a], Mahamoud Ali Chirdon[a], Moussa Mahdi Ahmed[a], Omar Assowe Dabar[a], Youssouf Djibril Soubaneh[c], Nima Moussa Egueh[a], Ali Dirir Kawalieh[a], Ibrahim Houssein Kadieh[d], Mohamed Chaheire[e]

[a]Institut des Sciences de la Terre. Centre d'Etudes et de Recherches de Djibouti (CERD). Route de l'aéroport. B.P. 486. Djibouti – ville. République de Djibouti.

[b]Department of Chemistry, Life Sciences and Environmental Sustainability, University of Parma, Parco Area delle Scienze 157/a, 43124 Parma – Italy.

[c]Département de biologie, chimie et géographie. Université du Québec à Rimouski. 300. Allée des Ursulines. Rimouski. QC. G5L 3A1. Canada.

[d]Laboratoire Régional, Newalta Châteauguay, 125 Rue Bélanger, Châteauguay, J6J 4Z2 Québec, Canada.

[e]Bureau Géologique des Comores, 8083-Moroni Hadudja, Comores.

Abstract

Within the East African Rift System (EARS), the complex Ali-Sabieh aquifers system, located in the south of the Republic of Djibouti, was overexploited and subjected to anthropogenic and/or geogenic pollution with high concentrations of dissolved nitrate (up to 181 mg/l) and sulfates (up to 1,540 mg/l).

This study is the first undertaken on the hydrochemistry of this aquifer system, combining geochemical tools and multi-isotope - $\delta^{2}H(H_2O)$, $\delta^{18}O(H_2O)$, $\delta^{18}O(SO_4)$, $\delta^{34}S(SO_4)$, $\delta^{15}N(NO_3)$, $\delta^{18}O(NO_3)$, $\delta^{13}C(DIC)$, and ^{14}C - was used to decipher the origin and fate of different nitrate and sulfate sources to groundwater.

The groundwater samples of the region show a chemical evolution from fresh Ca(Na)-bicarbonate to brackish Na-Cl, mainly due to water-rock interaction. The combined chloride and water isotope data show that evaporation and transpiration are present, with the latter occurring primarily in the shallow alluvial aquifer waters. Inspection of $\delta^{15}N(NO_3)$ vs. $\delta^{18}O(NO_3)$ and NO_3/Cl vs. Cl diagrams show that dissolved nitrates are primarily of anthropogenic origin. In particular, higher nitrate concentrations may be related to animal manure used as organic fertilizers during agricultural activities. Sulfates are from a natural origin related to the interaction of water with gypsum of hydrothermal or sedimentary origin. SO_4/Cl ratio and isotopic composition show that dissolved sulfates in saline and ancient groundwater of the Cretaceous sandstone aquifer (between 7.4 ± 2.2 and 5.8 ± 1.4 kilo-years before the present) are generated by interaction with gypsum from oxidation of pre-existing (Jurassic?) sulfides.

This work highlight that isotopic ratios of the two molecules – $\delta^{18}O(SO_4)$, $\delta^{34}S(SO_4)$, $\delta^{15}N(NO_3)$, $\delta^{18}O(NO_3)$ – are not sufficient for tracing the origin of nitrate and sulfates in groundwater, but that a complete hydrogeochemical study is needed. In the absence of this,

Formattato: Non Evidenziato
Formattato: Non Evidenziato
Formattato: Non Evidenziato
Formattato: Non Evidenziato
Formattato: Non Evidenziato
Formattato: Non Evidenziato
Formattato: Non Evidenziato
Formattato: Non Evidenziato
Formattato: Non Evidenziato
Formattato: Non Evidenziato

the relatively high concentration of chloride and sulfates could be wrongly linked to the anthropogenic source of nitrate (manure or sewage).

Keywords: Djibouti, Hydrochemistry, Radiogenic isotopes, Stable isotopes, Nitrogen isotopes; Sulfates isotopes

*Corresponding author. Tel: +253 77 84 68 55; awaleh@gmail.com

1. Introduction

The Republic of Djibouti is located in the Horn of Africa, which is an emerged triple junction of the Red Sea, the Gulf of Aden and the East African Rift (Fig. 1). As in other rifting zones, the activity of the EARS corresponds to large seismic, tectonic and volcanic activities (Barberi et al., 1975; Mlynarski and Zlotnicki, 2001). As a consequence of the tectonic activity in the rifting system, the level of complexity of the hydrogeological setting is highly variable in the EARS (Mechal et al., 2017). Therefore, the complexity of the aquifer systems in the Republic of Djibouti is a result of the heterogeneity of these aquifers combined with climate change impacts, and anthropogenic pressures (Awaleh et al., 2018).

Within the EARS, the Ali-Sabieh volcano-sedimentary aquifers system, located in the south-east of the Republic of Djibouti, faces increasing anthropogenic pressures due to the combined effects of population growth and persistent droughts, exacerbating already existing water quality and quantity. Additionally, the Republic of Djibouti has an arid climate with an average annual rainfall of less than 150 mm (Assowe et al., 2021). This harsh climate has led the country to overexploit the only available water sources, which are represented by groundwater in complex volcanic aquifers (Jalludin and Razack, 2004; Houssein and Jalludin 1996; Awaleh et al., 2017, 2018).

The complex Ali-Sabieh aquifers system provides drinking and irrigation water to the population in the Ali-Sabieh region (Fig. 1). The aquifers of Ali-Sabieh are also the most

Eliminato: Thirty-four groundwater samples from the Ali-Sabieh region are characterized for their dissolved major constituents, including fluoride and bromide, and the following isotopes: $\delta^{15}N(NO_3)$, $\delta^{18}O(NO_3)$, $\delta^{34}S(SO_4)$, $\delta^{18}O(SO_4)$, $\delta^{13}C(DIC)$, ^{14}C, $\delta^{2}H(H_2O)$, and $\delta^{18}O(H_2O)$. The water quality index is globally poor for the whole area. In addition to fluoride, which is generally present in large quantities in the waters of the East African Rift System (EARS), poor water quality is due to high concentrations of dissolved nitrate (up to 181 mg/l) and sulfate (up to 1,540 mg/l), as well as high salinity (up to 7 g/l) in the deeper Cretaceous sandstone aquifer. The waters of the region show a chemical evolution from fresh Ca(Na)-bicarbonate to brackish Na-Cl, mainly due to water-rock interaction. Combining the chloride and water isotope data shows that evaporation and transpiration are also present, with the latter occurring primarily in the shallow alluvial aquifer waters. Although the presence of desert/evaporitic nitrates (saltpeter) was assumed in a previous study, stable isotope ratios show that dissolved nitrates are primarily of anthropogenic origin. In particular, higher nitrate concentrations may be related to animal manure used as organic fertilizers during agricultural activities. Sulfates are from a natural origin and related to the interaction of water with gypsum of hydrothermal or sedimentary origin. In particular, chemical ratios of dissolved constituents (SO_4/Cl) and isotopic composition show that dissolved sulfates in saline and ancient groundwater of the Cretaceous sandstone aquifer (between 7.4 ± 2.2 and 5.8 ± 1.4 kilo-years before the present, inferred by different modeling using radiogenic and stable carbon isotopes) are generated by interaction with gypsum from oxidation of pre-existing sulfides (perhaps from the Jurassic era). ¶
The scarce number of studies on the origin of nitrate and sulfates in the waters of volcano-sedimentary aquifers in arid climates make this work a potential reference for future studies in similar areas worldwide. In particular, this work shows that isotopic ratios of the two molecules –$\delta^{18}O(SO_4)$, $\delta^{34}S(SO_4)$, $\delta^{15}N(NO_3)$, $\delta^{18}O(NO_3)$– are not sufficient for tracing the origin of nitrate and sulfates in groundwater, but that a complete hydrogeochemical study is needed. A complete study should include an analysis of the salinization mechanism and the possible mixing between aquifers. In the absence of this, the relatively high concentration of chloride and sulfates could be wrongly linked to the anthropogenic source of nitrate (manure or sewage).¶

exploited for agriculture purposes in the country. Therefore, knowledge of the origin of groundwater resources, their renewal forms, and the consideration of their vulnerability facing the anthropogenic pressure is essential to the rational management of this complex volcano-sedimentary aquifers system. However, excluding the report on some physico-chemical parameters of irrigation water carried out by JICA (2014), to the best of our knowledge, no in-depth hydrogeochemical study has been carried out so far on this complex volcano-sedimentary aquifers system.

Nitrate concentrations in water above the World Health Organization (WHO) guideline value (50 mg/l) and especially when above 100 mg/l, often in the presence of gastrointestinal infections, can cause health problems such as methemoglobinemia (WHO, 2011). Although the human health effects of high sulfate concentrations are not yet apparent, the Environmental Protection Agency (EPA) and the WHO have set thresholds for sulfate concentrations below 1,000 mg/l in drinking water at 250 (EPA, 2003a) and 500 mg/l (WHO, 2004), respectively. Indeed, infants may experience gastroenteritis, with symptoms including diarrhea and dehydration, the first time they ingest water containing high concentrations of sulfates (Backer et al., 2001). Changing water sources or using bottled water is often recommended to manage the risk (EPA, 2003b), which can be difficult to implement in developing countries.

The dual isotopic composition of dissolved nitrate in waters, $\delta^{15}N(NO_3)$ and $\delta^{18}O(NO_3)$, has been used extensively to better constrain the sources of nitrate in groundwater (Kendall, 1998; Kendall et al., 2007). However, there are few studies on the origin of the high nitrate content of groundwater in semi-arid or arid areas around the world using dual nitrate isotopes (Edmunds and Gaye, 1997; Jackson et al., 2015; Stadler et al., 2008; Walvoord et al., 2003; Awaleh et al., 2017, 2018).

This study is the first on the hydrochemistry of this complex volcano-sedimentary aquifers system. The geochemical and environmental studies of sulfate and nitrate pollution processes are often limited to the analysis of the concentration and to the isotopic ratio of one or both molecules of interest (e.g., Rock and Mayer, 2002; van Dijk et al. 2019) or extended to major chemical-dissolved constituents and water isotopes (e.g., Torres-Martínez et al. 2021). In this study, environmental and radiogenic isotopes, $\delta^{2}H(H_2O)$, $\delta^{18}O(H_2O)$, $\delta^{18}O(SO_4)$, $\delta^{34}S(SO_4)$, $\delta^{15}N(NO_3)$, $\delta^{18}O(NO_3)$, $\delta^{13}C(DIC)$, and ^{14}C, as well as major ion chemistry combined with geological, tectonic and regional hydrogeology information are applied to assess the geochemical evolution and groundwater residence times of the Ali-Sabieh aquifers system.

The goals of this study are: (1) to characterize the main geochemical processes that explain the waters geochemistry of the Ali-Sabieh aquifers system and to understand their geochemical evolution and groundwater residence time, (2) to track the origin and fate of the nitrate in groundwater from these aquifers, and (3) to decipher the origin of the very high sulphate contents in groundwater from these aquifers. The results obtained will contribute to a comprehensive knowledge of the Ali-Sabieh aquifers and will be helpful for planning future management of this complex hydrological system of the EARS. Further, this study will serve as a valuable base for other integrated geochemical and isotopic studies of volcano-sedimentary aquifers in similar arid environments.

2. Site description

2.1 Climate and hydrogeological settings

The Köppen and Geiger climate classification of the area ranges from "hot desert" to “semi-arid” (climate type codes BWh and BSh, respectively) (Beck et al., 2018; Geiger, 1954). The Republic of Djibouti has a low precipitation regime, with an annual rainfall range of 60–300 mm (Assowe et al., 2021). Rainfall variation in the Republic of Djibouti is embedded in large-

scale climate variability, particularly when there is El Niño Southern Oscillation and Indian Ocean Dipole IOD (Assowe et al., 2021). The two predominating seasons are a cool season (winter) from October through April and a hot season (summer) from May through September. In winter, the climate is characterized by northeast trade winds coming from Saudi Arabia and the Gulf of Aden and an average temperature between 20°C and 30°C. In summer, an equatorial westerly wind zone dominates (Assowe et al., 2019), and average temperatures range from 30°C to 45°C with a high evapotranspiration rate amounting to 2,000 mm per year (BGR, 1982). The aridity of the climate is further enhanced by a particularly hot and dry westerly wind regime (known as khamsin) resulting from the warming and drying of the East African monsoon (the foehn effect) as it blows over the mountain ranges of Somalia and Ethiopia. Because of this arid climatic regime, most watercourses in the Republic of Djibouti are temporary and run for only a few hours after any rain event (wadis).

The study area is localized in four endorheic watersheds, namely the Deydey Weyn watershed, the Beyya Dader watershed, the Beyya Aday watershed, and the Barislé watershed (Fig. S1; Table S1 in Supplementary Material). The groundwater in the Republic of Djibouti is controlled by volcanic and sedimentary aquifers. Volcanic aquifers are mainly represented in the study area by the Somali basalt, the Dalha basalt, the Ali-Sabieh rhyolites, and the Ali-Sabieh sandstone (from the Cretaceous area) (BGR, 1982). The Ali-Sabieh aquifer systems are composed of two aquifers: (i) the inferoflux (shallow) aquifer and (ii) the deep volcanic/sedimentary aquifer (BGR, 1982). Shallow alluvial/sedimentary aquifers (inferoflux) are mainly located in the wadi beds, while the deep sedimentary (sandstone cretaceous) aquifer is located in the Ali-Sabieh city area (Fig. 1). It has been reported that the groundwater flow in the study area is from the southwest to the northeast and from the west to the east (Fig. S1 in Supplementary Material, BGR, 1982). The transmissivity of the Dalha basalt, the Somali basalt and the Ali-Sabieh rhyolites ranges between 1.5 x 10^{-3} m^2/s and 2.4

x 10^{-3} m^2/s, 1.3 x 10^{-2} m^2/s and 2.1 x 10^{-2} m^2/s, and 3.5 x 10^{-5} m^2/s and 1.7 x 10^{-3} m^2/s respectively (Jalludin and Razack, 2004).

2.2 Geological setting

Djibouti has recorded one of the complete volcanic stratigraphy successions of the Afar rift system, dating back about 30 Ma. The earliest synrift volcanics are the 28-20 Ma-old Ali Sabieh mafic series (both effusive and intrusive) that rest over the Meso-Cenozoic sedimentary substratum terranes in the Ali Sabieh antiformal area (Le Gall et al., 2010). They are overlain by the more extensive, 19-11 Ma-old Mablas felsic lavas that consist of rhyolites, ignimbrites and minor basaltic lava flows, intruded by felsic dykes and the tilted Dalha basalts, in which about 1,000 m of basaltic flows erupted at 9–4 Ma, just before the initial opening of the Tadjoura Gulf (Gadalia, 1980; Gasse et al., 1986; Audin et al., 2004). These basalts are correlative with the Somali basalts emplaced approximately during the same period of time (7.2–3 Ma) (Audin et al., 2004). At around 3 Ma, a significant kinematic change occurred in the Afar rift system and was expressed by the emplacement of the 3–1 Ma Stratoid trap-like basalts that floored the Afar Triangle (Varet and Gasse, 1978), and the westward propagation of the Gulf of Aden accretionary axis through the Tadjoura rift and its onshore prolongation to the NW along the Asal axis (Manighetti et al., 1998). The Asal rift is usually regarded as a nascent slow-spreading ridge (Stieltjes, 1973; Barberi et al., 1977; Pinzutti et al., 2013).

The study area is located in the Southern part of the country, and the Ali Sabieh anticlinal structure is mainly composed of intrusive mafic sequences, Jurassic limestones and Cretaceous sandstones. The latter are overlain by effusive basaltic sequences and the Mablas acidic series (15–11Ma). The Dalha (8.6–3.8 Ma) form the western flank while the Somali basalts lava flow characterizes the eastern part. The Jurassic limestones and basaltic

sequences are affected by NW-SE faults. They are also intruded by sill/dyke swarms with predominant NE-SW and N-S orientations (Le Gall et al., 2010). The Dahla basalts are affected by two distinct sets of faults at N160–180°E, crosscut by E-W faults-fractures and to a lesser extent N110–130°E croscutted by NS and N60–70°E directions. The western part of this area is characterized by the presence of (i) two sedimentary basins (Petit Bara and Grand Bara) and (ii) the Stratoid basalts (Arthaud and Jalludin, 1993).

2.3 Land use, farmland extension and crop fertilization

In the Ali-Sabieh region (2,200 km^2), farmlands were confirmed in Assamo, Hollholl, Faradil, Hambokto, Ali Adde, and Doure. Due to their low income, the people in these areas practice agropastoralism in order to increase food security and household income. Water from the inferoflux aquifer allows crops to develop along the banks of the wadis, hence the establishment of farms along the slope of the wadis to extract water for irrigation and for the consumption of their animals (Fig. S2 in Supplementary Material). The practice of surface irrigation is predominant compared to drip irrigation. However, the size of the total farmlands of each area is relatively small, with a total extension of 750,000 m^2 (JICA, 2014). This is mainly due to the arid/desert climate and reflects the general trend in the country. For a potentially cultivable area of 120,000 ha, the country has only about 10,000 ha of arable land, of which only 1,000 ha (i.e., 1%) is cultivated along the wadis (MAEPH, 2000). Therefore, the size of the farmland is conditioned by the areas where irrigation water exists. Although chemical fertilizers and pesticides are available in Djibouti City, they are only used in lands around the capital city (Damerjog, Douda, Atar, etc.). In rural areas, farmers traditionally use natural compost produced from goat, sheep, or camel manure due to their low cost and availability. Therefore, farmers use manure as fertilizer for their crops (tomatoes, onions, melons, dates, sorghums, moringas, guava fruits, etc.) (Fig. S3 in Supplementary Material).

JICA (2014) has inferred a total requested amount of 2,000 kg of manure per 10,000 m^2 as part of the Republic of Djibouti's agricultural master plan. However, there is no actual data on the exact amount of compost used in farmlands in the study area. This is probably due to the fact that farmers are mostly illiterate and do not keep records of the amount of manure used on their crops. Compost comes primarily from goats, which are the most widely distributed livestock in the Republic of Djibouti. Dung is collected in common manure pits and then mixed with a large amount of water up to a complete fermentation (JICA, 2014; Fig. S4 in Supplementary Information).

3. Material and methods

3.1. Sampling and field measurements

Water from nine boreholes and twenty-five hand-dug wells was collected in October 2020. Temperature (±0.1 ºC), pH (±0.01 unit), electrical conductivity (±1µS/cm), redox potential (±0.1 mV), and dissolved Oxygen (±0.1 mg O_2/l) were measured on-site using portable instruments. Specifically, CheckTemp (Hanna), pH 610 (EutechInstruments), COND 610 (Eutech Instruments), WTW Multi 3410, and YSI 550ADO Instruments were used, respectively. The instruments were calibrated in the field prior to measuring, with the exception of the YSI 550ADO instrument which was calibrated 24 hours prior to field sampling. Water samples were collected into polyethylene bottles after filtration through 0.45 µm membrane filters (Baird et al. 2017; Mortimer et al. 2014). All samples used for determination of cations were acidified after collection through the addition of Suprapur® HNO_3 (Merck) to bring the pH below 2 and stored at low temperature of 4°C as prevention of metabolism by microorganisms and aggregation of dissolved constituents (precipitation, flocculation, and complexing) (Baird et al. 2017; Mortimer et al. 2014; Śliwka-Kaszyńska et al. 2003).

3.2. Chemical analyses in laboratory

The analysis of major anions and cations was carried out at the CERD Laboratory using a Dionex ICS 3000 Ion chromatography using a Dionex Ionpac AS-9HC and a CS12A columns (4mm×250mm), respectively, following the manufacturer's procedures, and Chromeleon Software Version 6.8 (Dionex, Suunyvale, CA, USA) following ISO 14911 (ISO, 1998) and ISO 10304 (ISO, 2007). Quality assurance measures included an initial calibration, which was monitored throughout the analysis via checks and spikes, and sample triplicates (10% frequency). The certified reference materials used are the primary multi-cation (Sigma Aldrich, 89886) and multi-anion solution (Sigma Aldrich, 89316), both with an expanded uncertainty of 0.02 mg/l. Calibration check criteria were: recovery 90 – 110%, precision ±10% and spike recovery 80 – 110%. All sample runs met these conditions. HCO_3 was analyzed for by titration with 0.1 M HCl following Gran method. The correctness of the water chemical analyses was checked in agreement with the Standard Method 1030E (Baird et al., 2017). In particular, the charge balance between anions and cations was assessed and analyses were accepted if deviation were equal or below 5%.

3.3. Isotope measurements

Additional samples of untreated waters were collected into 50 mL glass bottles (Quorpak) for analysis of the hydrogen and oxygen stable isotope ratio of the water molecule, $\delta^2H(H_2O)$ and $\delta^{18}O(H_2O)$, respectively. Water samples filtered through 0.45 µm membrane filters were collected into 1000 mL Nalgene bottles for the analysis of radiocarbon activity (^{14}C), and into 500 mL plastic bottles for the carbon stable isotope ratio determinations of dissolved inorganic carbon $\delta^{13}C(DIC)$.

289 The isotope ratios of hydrogen and oxygen of the water molecules were analyzed at the
290 Environmental Isotope Laboratory at the University of Waterloo (in Canada) using a Los
291 Gatos Research (LGR) Liquid Water Isotope analyser (LWIA), model T-LWLA-45-EP
292 instruments, and they were converted in per mil delta values (δ ‰) versus the Vienna
293 Standard Mean Ocean Water (V-SMOW) standard following δ (‰) = [(R_{sample} / $R_{standard}$) - 1]
294 x 10^3, where R is the isotopic ratio of interest ($^2H/^1H$ or $^{18}O/^{16}O$). The average precision,
295 based on multiple analyses of various samples and laboratory standards was ± 0.2‰ for
296 $\delta^{18}O(H_2O)$ and ± 0.8 ‰ for $\delta^2H(H_2O)$. The ^{13}C ratios were determined using a mass
297 spectrometer (a Micromass, Isoprime model with triple universal collectors) at the
298 Environmental Isotope Laboratory at the University of Waterloo (Canada). $^{13}C/^{12}C$ ratios are
299 reported using the conventional δ (‰) notation as a deviation from the V-PDB standard, and
300 the error for $\delta^{13}C$(DIC) is ±0.2‰ (the mean error was obtained from replicate analyses). For
301 the ^{14}C activity, the Environmental Isotope Laboratory at the University of Waterloo (Canada)
302 converts the groundwater samples to pure carbon dioxide which is trapped in 6 mm OD Pyrex
303 glass tubes (Breakseal) that are then send to various Accelerator Mass Spectrometry labs
304 around the world for ^{14}C determination. Carbon dioxide is reduced to graphite according to
305 strictly defined protocols. Graphitized samples are measured on a state-of-the-art National
306 Electrostatics Corporation 1.5SDH-1 Pelletron Accelerator. The ^{14}C results were reported as
307 percent Modern Carbon (pMC) with an average 1σ error of ±0.3 pMC.
308 Samples for sulfur and oxygen isotope analyses were collected using 250 mL pre-acid-washed
309 plastic perplex bottles. To precipitate reduced sulfur as CdS, Cd-acetate was already added in
310 the bottles (5% v/v) prior to sample collection and then the aliquot was filtered through a 0.2
311 μm nitrocellulose filter before chemical determination of residual sulfate. Then, dissolved
312 sulfate was precipitated as $BaSO_4$ at pH < 4 (in order to remove carbonate and bicarbonate
313 species) by adding a $BaCl_2$ solution. The isotopic analyses on $BaSO_4$ were carried out using

314 an IsoChrom Continuous Flow Stable Isotope Ratio Mass Spectrometer coupled to a Carlo
315 Erba Elemental Analyzer at the Environmental Isotope Laboratory at the University of
316 Waterloo (Canada). Sulfate-isotope compositions, $\delta^{34}S(SO_4)$ and $\delta^{18}O(SO_4)$, were reported in
317 the usual δ-scale in ‰ with reference to V-CDT (Vienna Canyon Diablo Troilite) and V-
318 SMOW (Vienna Standard Mean Ocean Water), with a precision of ±0.3‰ and ±0.5‰,
319 respectively.
320 The $\delta^{15}N(NO_3)$ and $\delta^{18}O(NO_3)$ values were measured at the University of Waterloo
321 Environmental Isotope Laboratory (Canada). Each sample is prepared in duplicate and
322 analyzed as independent sample. NO_3^- is converted to NO_2^- using a cadmium catalyst then
323 chemically converted to N_2O. The converted gas is then analyzed for $\delta^{18}O$ and $\delta^{15}N$ utilizing
324 an Isoprime Trace Gas continuous flow mass spectrometer (from GV Instruments,
325 Manchester, UK) (McIlvin and Altabert, 2005; Spoelstra et al., 2014). Isotopic ratios are
326 reported in delta (δ) notation in units of per mil (‰) relative to the reference standards of
327 atmospheric N_2 for $\delta^{15}N(NO_3)$ and VSMOW for $\delta^{18}O(NO_3)$. Three calibrated standards,
328 USGS34, USGS35 and in house EGC 17 are used for normalization. Also included in each
329 batch are three check standards at the start middle and end. Two are in house EGC 1 and a
330 single IAEA NO-3. During a sample run, linearity checks are included using a suite of 100
331 ppm N_2O in helium of known isotopic composition to produce a range of peak heights that
332 encompass the expected sample peaks range. The analytical precision for $\delta^{15}N(NO_3)$ and
333 $\delta^{18}O(NO_3)$ values are ±0.5‰ and ±1.0‰, respectively.
334
335 *3.4. Thermodynamic calculations and isotope-mass balances*
336 The mean values of mineral saturation indices and the partial pressure of the dissolved carbon
337 dioxide as $\log PCO_2(g)$ were calculated by the values obtained from PHREEQCI Version 3
338 (Parkhurst and Appelo, 2013) and The Geochemist's Workbench® version 12 (Bethke et al.,

2016) codes using *thermo.com.v8.dat* and *thermo.dat* thermodynamic datasets, respectively. The use of two codes and datasets allows for knowing the error on the values obtained, which depends on different methods of the calculation of the activity coefficients (Debye-Hückel and B-Dot; Bethke, 2008) and the uncertainty on the thermodynamic data. Finally, the NetpathXL code, Version 1.5 (Parkhurst and Charlton 2008; Plummer et al., 1994) and the physico-chemical composition of the samples were used to calculate the $\delta^{13}C(CO_2)g$ values from $\delta^{13}C(DIC)$ and to calculate and correct the radiocarbon dating of groundwater from ^{14}C data using an isotope-mass balance approach (Clark and Fritz, 1997).

3.5. Water quality indices

To have a comprehensive picture of the chemical quality of groundwater, the weighted water quality index (wWQI) was used (Horton, 1965; Brown et al., 1970; Brown et al., 1972). Guideline values of the pH, total dissolved solids (TDS), nitrate, fluoride, chloride, sulfate as published by the EPA (2021) and the WHO (2021) were used as references. A weight *wi* was assigned to the chemical parameters according to their relative importance in the overall quality of groundwater for drinking purposes. The maximum weight 5 was assigned to nitrates and fluorides because of their importance in drinking water quality and the well-known health risk associated with high concentrations; a weight 4 was assigned to sulfates, chlorides and TDS because of their potential taste and palatability issues; the minimum weight of 2 was assigned to pH and sodium because their objective concentrations are defined as "aesthetic" (WHO, 2011). Then, the *wWQI* was calculated for each groundwater sample as follow:

$$wWQI = \sum Wi \times qi = \sum \left[\left(\frac{wi}{\sum qi} \right) \times \left(\frac{V_i - V_{min}}{V_{max} - V_{min}} \times 100 \right) \right], \quad (1)$$

where W_i is the relative weight of ith parameter; qi is the water quality rating; *Vi*, V_{min}, and V_{max} are the concentration value in the sample and the minimum and maximum suggested by the WHO and/or the EPA for that parameter, respectively. For example, a concentration of 1.5 mg/l (V_{min}; WHO, 2021) and 4.0 (*Vmax*; EPA, 2021) are actually suggested for fluoride. According to Batabyal and Chakraborty (2015), five quality grades were defined to classify the results obtained from the *wWQI* calculation. Since the weights attribution is subjective, the values obtained were also compared with the Canadian Water Quality Index (*CWQI*) (CCME 2001; CCME 2017), using the SS-WQI 1.0 spreadsheet (https://www.gov.nl.ca/ecc/waterres/quality/background/ss-wqi/) and the same guideline values used to calculate the *wWQI* index. Rather than calculating an index value for each water sample as the *wWQI*, the *CWQI* provides an overall water quality of the studied area (Davies, 2006).

4. Results and discussion

Groundwater samples were separated into five categories based on geographic location, and the type of aquifer tapped by the boreholes and hand-dug wells, which are: (1) Transboundary Basalt Aquifer (TBA) boreholes (i.e. borehole #1, in the Galile area); (2) Ali-Sabieh Sandstone (Cretaceous) Aquifer (ASGA) boreholes (i.e. boreholes #2–#4, in the Ali-Sabieh City area); (3) Ali Sabieh Basalt Aquifer (ASBA) boreholes (i.e. borehole #5, in the Faradil area); (4) Dalha Basalt Aquifer (DBA) boreholes (i.e. borehole #6, in the Doure area); and (5) Somali Basalt Aquifer (SBA) boreholes (i.e. borehole #8 and #11, in the Hindi–Holl-Holl area). The hand-dug wells all tap the superficial alluvial aquifers located in the wadi beds of the study area (Table S2). For the sake of simplicity, in the following figures, the samples are represented with three different colors indicating the lithology (red represents basalts; yellow represents sandstone, and green represents alluvium).

4.1 Groundwater geochemistry

The temperature, pH, EC, E_h, O_2, total dissolved solids concentrations (TDS), and sampling locations are given in Table S2 (in Supplementary Material). The physico-chemical parameters and the isotope data of the groundwater samples from the study area are reported in Table 1. Classification of the water samples in Table S2 were made according to the dominant cation and anion (meq/l), which coincides with was calculated by the Geochemist's Workbench® code. The pH values of groundwater samples in the study area range from 7.03 to 8.87, indicating neutral to alkaline characteristics. Groundwater had low to high EC values ranging from 355 to 7259 µS/cm. According to the classification of water based on TDS (Kharaka and Hanor, 2014), 82% of the groundwater in the study area is brackish (10 g/l > TDS > 1 g/l), while 18% is fresh (TDS < 1 g/l) (Table S2). Brackish waters are mainly Na-Cl, Ca-Cl and Na-SO_4, while freshwater waters are Na-HCO_3 and Ca-HCO_3 type (Table S2).

The Langelier–Ludwig diagram is a key plot in showing the evolution of the chemical composition of groundwater (Langelier and Ludwig, 1942; Boschetti, 2011). From this plot, one can observe that freshwaters shift towards the Na-HCO_3 and Ca-HCO_3 corner, as is typical for wadi-recharged aquifers (Awaleh et *al.*, 2017; Awaleh et *al.*, 2018) (Fig. 2). In contrast, most of the borehole groundwaters are mainly clustered in the upper left alkali-chloride-sulfate sub-square of the diagram (Fig. 2). The distribution described above is also illustrated by the water samples collected by JICA (2014) in the Ali-Sabieh region. Further, the clustering of some samples near the seawater point may suggest marine ingression in this area, or the presence of fossil water of similar origin. However, it should be noted that the deep waters may have had a hydrothermal origin or some degree of mixing with this kind of water, as has also been demonstrated in other areas of the country (Awaleh et al., 2015a; Awaleh et al., 2017; Awaleh et al., 2020). In this regard, the most representative waters of

412 hydrothermal origin from the previously mentioned studies are also drawn in Fig. 2. The
413 brackish samples collected in this study are mainly displaced between the vertical line of the
414 fresh-brackish switch and the hydrothermal waters fields (Fig. 2), as has also been
415 demonstrated for groundwater in the Bara desert area (the Dikhil and Arta Regions are the
416 light gray field in Fig. 2) (Awaleh et al, 2017a). Only the two Ca-Cl samples are significantly
417 shifted in the lower left earth-alkaline-chloride-sulfate sub-square of the diagram (Fig. 2),
418 probably due to a Na-Ca cation exchange effect. Regarding the calculated saturation indices,
419 almost all groundwater is oversaturated with respect to carbonate minerals (calcite, aragonite
420 and dolomite) and undersaturated with respect to anhydrite, gypsum, and halite (Table S3, in
421 Supplementary Information). In most groundwater samples, the Ca/SO_4 ratio is less than one,
422 with the exception of two boreholes (#6 and #8), and eight hand dug wells (#16, #17, #19,
423 #20, #25, #29, #37, and #38) where the ratio is greater than one (Table S4, in Supplementary
424 Information). On the other hand, most groundwater in the study area has a Ca/HCO_3 ratio
425 greater than one (Table S4). Almost all groundwaters is oversaturated with respect to
426 carbonate minerals, and the excess calcium in these groundwaters (i.e. $Ca/SO_4 > 1$ or
427 $Ca/HCO_3 > 1$) should probably resulted from the weathering of anorthite, which is evident in
428 the chemical composition of Dalha basalt (Gasse et *al.*, 1986).
429 Na-excess is the main feature of the fresh groundwater in the study area, as also revealed by
430 the Na/Cl ratio (Table S4). The equivalent basis ratio $Na/Cl > 1$ in these groundwaters (Table
431 S4) may indicate that a large fraction of the sodium is associated with an anion other than
432 chloride. In other words, the Na/Cl equivalent basis ratio greater than one is generally
433 interpreted as reflecting the release of the sodium ion from silicate weathering reactions
434 (Meybeck, 1987). Therefore, a potential source of Na^+ excess could be the alteration of sodic
435 plagioclase (e.g. albite), which is significantly present in the volcanic rocks (Dalha Basalt) of
436 the south of the Republic of Djibouti (Aboubaker, 2012). Another feature is the enrichment in

magnesium relative to calcium (Ca/Mg < 1) in some of the groundwater samples (Table S4). Most of the groundwater in the study area has a Mg/HCO_3 ratio greater than one (Table S4). The enrichment in magnesium relative to calcium in these waters can be related to the weathering of a mafic mineral such as biotite or olivine (Aboubaker et *al.*, 2013).

The EARS hosts the most severe fluoride belt in the world (Chowdhury et al., 2019). Therefore, occurrences of elevated fluoride levels in groundwater within or close to the EARS are observed. Some groundwaters in the study area have a fluoride concentration higher than the 1.5 mg/l concentration limit for drinking water (WHO, 2021). Therefore, the risk linked to chronic fluorosis from these waters, which are used for human consumption by the local population is similar to that reported for other areas of the EARS (Gupta and Ayoob, 2016). The cause of the high fluoride concentration in EARS waters is related to low calcium concentration in solutions and interaction with fluorite, which could be present in sedimentary and volcanic formations, and which is more soluble than other fluoride-bearing minerals (Caminiti, 2015; Gizaw, 1996; García and Borgnino, 2015). In addition, the Ca^{2+} fixation by carbonate minerals, including cation exchange processes, could enhance the fluorite undersaturation and increase the concentration of dissolved fluoride during the geochemical evolution of the water (Awaleh et *al.*, 2020; Darling, 1996; Gizaw, 1996).

The plot of $[(Ca^{2+} + Mg^{2+}) - (HCO_3^- + SO_4^{2-})]$ versus $(Na^+ - Cl^-)$ has been widely used to illustrate the possibility of cation exchange in groundwater (Fisher and Mullican, 1997; Jankowski et al., 1998; Awaleh at al., 2018). In this plot, all groundwaters in the study area show a negative linear correlation with a slope of −1, demonstrating that cation exchange between Na^+, Ca^{2+} and Mg^{2+} has occurred in these waters (e.g., Awaleh at al., 2018) (Fig. S5, in Supplementary Information). However, it should be noted that in the EARS, sodium is not only related to chloride, but also to bicarbonate due to the interaction between dissolved CO_2 and sodium-bearings silicates (albite, analcime, etc.) (Awaleh et al., 2015a; Kebede, 2013).

Therefore, such an interpretation should be taken with caution and further diagrams are needed to confirm the hypothesis of cation exchange. For this purpose, the molar relationship between Ca and Na was also inspected. Most of the groundwaters are displaced between the highest TDS and calcium groundwater samples from Ali-Sabieh boreholes and the 1Ca – 2Na lines (Fig. S6, in Supplementary Information). Na-SO_4 and Ca-Cl waters are shifted towards these lines; in particular, the latter could have originated from Na-Ca substitution in Na-Cl water after an interaction with Ca-enriched clays (Fig. S6, in Supplementary Information). Indeed, cation exchange processes can be expressed as follows:

$$Ca^{2+}\,(Mg^{2+}) + 2NaX \rightarrow 2Na^{+} + Ca(Mg)X_2 \quad (2)$$

$$Ca(Mg)X_2 + 2Na^{+} \rightarrow Ca^{2+}\,(Mg^{2+}) + 2NaX \quad (3)$$

The chloro-alkaline CAI1 ($[(Cl^-) - (Na^+ + K^+)]/Cl^-$) and CAI2 ($[(Cl^-) - (Na^+ + K^+)]/(HCO_3^- + CO_3^{2-} + SO_4^{2-} + NO_3^-)$) indices were also applied to analyze cation exchange (Schoeller, 1977) (Table S4, in Supplementary Information). Negative values of the two indices could be obtained by cation exchange expressed as Eq. (2), while positive values of the two indices suggest the occurrence of cation exchange expressed as Eq. (3). The CAI1 and CAI2 varied from −1.23 to 0.45 with a mean of −0.11 and from −0.54 to 0.71 with a mean of +0.06, respectively, indicating the occurrence of cation exchange of Na^+ (and in minor amounts K^+) in the sediment with Ca^{2+} and Mg^{2+} in the groundwater (for example, in the alluvial aquifer).

4.2 Water quality indices

The water quality indices provide similar results by classifying the studied groundwater quality studied as "poor" despite the difference in calculation method (Supplementary File WQIs). In fact, using the weighed water quality index wWQI, which provides a rating value

for each sample, most groundwater samples (38%) have a “Poor” rating. Apparently, lithology is not related because both basaltic and alluvial aquifer waters are included in this category. In fact, these waters have high concentrations of both nitrates and fluorides. In addition, despite its very low nitrate concentration, the groundwater of the Ali-Sabieh sandstone aquifer has the worst rating ("unsuitable"), mainly because of its very high salinity and sulfate concentration. All freshwater samples have the highest rating (excellent). Like the *wWQI*, the *CWQI* index, which offers a general index without values associated with a single sample, provides a value of 42. This corresponds to the same "Poor" quality classification, with 41% of the samples not meeting guideline values (Supplementary File WQIs).

4.3. Water isotope composition: aquifer recharge and groundwater flow pattern

The oxygen $\delta^{18}O(H_2O)$ and hydrogen $\delta^{2}H(H_2O)$ ratios are useful tracers for determining the origin of groundwater and are widely used in studying natural water circulation and groundwater movement. However, in Djibouti, the mixing effect, groundwater flow, and isotope differentiation of aquifers in Djibouti are masked by the wide deuterium excess range of the local meteoric water line (Awaleh et al., 2020).

In Fig. 3, all data is compared with the Global Meteoric Water Line (GMWL) $\delta^{2}H(H_2O) = 8 \times \delta^{18}O(H_2O) + 10$ as defined by Craig (1961) and with the Local Meteoric Water Line (LMWL) as defined by Fontes et al. (1979). The LMWL has the same slope as the GMWL and a deuterium excess of $d = 2$. It should be noted that the LMWL is the most probable orientative proxy of the isotopic composition of local precipitation, although it cannot be used as an absolute reference for evaporative effects.

The stable isotope composition of groundwaters from the study area show that $\delta^{18}O(H_2O)$ values range from −2.79‰ to −0.61 ‰, whereas $\delta^{2}H(H_2O)$ values range from −13.6‰ to +1.12‰ (Table 1). Therefore, stable water isotope compositions for all groundwater samples

512 indicate a meteoric origin for recharge. The groundwater from Ali-Sabieh sandstone shows
513 the most depleted values, which might be related to the contribution of older (paleo?) water
514 recharge (Awaleh et al., 2017a).
515 All hand-dug well in the study area (i.e., within the range of wadi-recharged aquifers in the
516 Republic of Djibouti) have $\delta^{18}O(H_2O)$ and $\delta^{2}H(H_2O)$ values ranging from −2.07‰ to −0.63‰
517 and from −5.88‰ to +1.12‰, respectively (Fontes et al., 1980; Bouh, 2006; Awaleh et al.,
518 2017, 2018) (Fig. 3). The best fit line for the isotopic data of the alluvial aquifer waters shows
519 a slope of 4.4. The latter is consistent with the path drawn mainly by water samples from the
520 alluvial aquifer (Schoell and Faber, 1976; Bouh, 2006; Awaleh et al., 2018), which usually
521 show ^{2}H and ^{18}O isotopic enrichment on the right side of the waterline and with a slope (S ~
522 5) typical of arid climate at this latitude, indicating evaporative enrichment (Kebede, 2013)
523 (Fig. 3). The combined use of stable isotopes with the chloride concentration of water is a
524 powerful tool for verifying mixing between water masses of different salinities and, therefore,
525 for tracing the origin of the salinity (Fritz and Fontes, 1989; Fontes and Edmunds, 1989;
526 Boschetti et al., 2015). The chloride versus water isotope plots reveal that groundwater from
527 the Dahla and Ali-Sabieh basalt may result from mixing between two end-members: (i) Ali-
528 Sabieh sandstone groundwater (#3, #4) and (ii) Somali basalt groundwater (#7, #8) (Fig S7,
529 see supporting information). Borehole #1 is located in Galilé, southwest of the study area, on
530 the Djibouti-Ethiopia border. According to the groundwater movement in the study area,
531 groundwater flows from the southwestern part of the study area (the Galilé area) to the
532 northeastern part (the Hindi – Holl-Holl area) (Fig. S1). Therefore, an interconnection
533 between deep aquifers would be possible.
534 Plots of stable isotope values versus Cl^- concentration in alluvial and basalt aquifer waters
535 demonstrate that most of these waters show almost no sign of increased Cl^- concentration
536 during evaporation (Fig. S7, in Supplementary Material). It should be noted that most of the

alluvial waters in this region are used for irrigation purposes, with fruit trees such as guava that may account for this transpiration. Thus, plant transpiration is probably one of the processes of solute concentration in these waters (Fig. S8, in Supplementary Material). However, it is difficult to evaluate whether mineral dissolution/transpiration occurred before or after evaporation using a deuterium excess versus TDS diagram (Huang and Pang, 2012) (Fig. S8, in Supplementary Material).

Somali basalt groundwater in the Hindi–Holl-Holl area (i.e. boreholes #7 and #8), in the northeastern part of the study area, has stable isotopes similar to those of the local alluvial aquifer (i.e. hand-dug well #9) (Table 1) (Fig. 3). Therefore, it was mainly recharged from the local alluvial aquifer. Similarly, borehole samples from the Dahla (#6) and Ali-Sabieh (#5) basalts were also likely recharged by local alluvial aquifers because they have water isotope values in the range of local alluvial samples (Fig.3, Table 1) and show isotope enrichment similar to that of the inferoflux (Fig S8, in Supplementary Material). Indeed, deep volcanic aquifers in the Republic of Djibouti were recharged by the local alluvial aquifers mainly through major faults (BGR, 1982; Aboubaker et *al.*, 2013; Awaleh et al., 2017). It was also reported that only rainfall events more significant than 10 mm were likely to recharge the deep volcanic aquifer in Djibouti (BGR, 1982). Therefore, in the arid climate of the study area, evaporative enrichment must have a significant effect on isotopic composition during groundwater recharge, which occurs by slow seepage in fractured rocks.

4.4. Natural versus anthropogenic sources

4.4.1 Insight from Cl/Br ratios

The Cl/Br ratio has been used as a tracer to determine the origin and evolution of surface and groundwater (Alcalá and Custodio, 2008). Cl/Br ratios versus Cl concentration could reveal a separation of different water groups and thus help distinguish natural from anthropogenic

562 sources (Panno et al., 2006; Alcalá and Custodio, 2008). In Fig. 4, the water samples show a
563 mean Cl/Br molar ratio of 649 ± 199. This could suggest a marine origin, considering the
564 mean seawater ratio of 655 ± 4 suggested by Alcalá and Custodio (2008). At this latitude, the
565 Cl/Br ratio of seawater is significantly higher at up to 720 (Awaleh et al., 2015b), but it
566 remains in the range of groundwater values. It should also be noted that groundwater in
567 Djibouti tends to remain in the typical Cl/Br molar ratio of basalts (435 – 769; Möller et al.,
568 2016), in which geothermal waters in the area also fall (Awaleh et al., 2017a). The similar
569 halides ratio of the studied groundwater and geothermal waters agrees with the main chemical
570 composition trend observed in Fig. 2. Similarly, the Na-Cl and Na-HCO_3 freshwaters with Cl
571 < 100 mg/l fall within or close to the values of the Cl/Br ratio of "recharge waters" suggested
572 by Alcalá and Custodio (2008) (Fig. 4). Apart from this clear distinction, the problem arises
573 for waters with higher chloride values, which cannot be unequivocally defined using the range
574 of Cl/Br ratios proposed in the literature. For example, groundwater from basalt aquifers falls
575 within the septic waste ratio suggested by Alcalá and Custodio (2008). However, septic
576 wastes with higher Cl/Br values have also been published (Panno et al., 2006; Rotiroti et al.
577 2017; Vengosh and Pankratov, 1998); in particular, the mean Cl/Br molar ratio of 2624
578 proposed for the Midwestern United States, has a wide range from 146 to 12159 that
579 encompasses both all of the samples in this study and most of the proposed anthropogenic
580 source ratios (Fig. 4). Animal manure also shows very different Cl/Br molar ratios: from 161
581 for goats (Hudak, 2003) to 3205 for hog and horse manures (Panno et al., 2006). The lower
582 ratios detected in manure leachate by Hudak (2003) could likely be due to several reasons
583 (drinking water and feed in different regions), including organic degradation (McArthur et al.,
584 2012) (Fig. 4). In any case, the use of Cl/Br ratios is not very useful in distinguishing
585 anthropogenic sources for this study area.
586

4.4.2 Origin of nitrate

All boreholes and hand-dug wells in the study area are used for drinking and/or irrigation purposes, although in some cases NO_3^- concentrations lie above the maximum permissible value prescribed by the World Health Organization for drinking waters (50 ppm; WHO, 2011; see Table1).

The isotope composition of nitrate molecules, $\delta^{15}N(NO_3)$ and $\delta^{18}O(NO_3)$, can be used for the identification of nitrate sources in groundwater (Kendall, 1998). To attribute each sample to a possible nitrate source, isotopic compositions were plotted in the classical $\delta^{18}O(NO_3)$ vs $\delta^{15}N(NO_3)$ diagram along with nitrate sources from the literature (Fig. 5). The $\delta^{15}N(NO_3)$ values of the study area water samples with higher nitrate concentration ranged from +10.7‰ to +15.6‰ while $\delta^{18}O(NO_3)$ values of these waters ranged from +7.5‰ to +14.8‰ (Table 1, Fig. 4). Based on published N-isotope ranges (Kendall, 1998; Kendall et al., 2007; Aravena and Mayer, 2010), all groundwater with high nitrate concentrations is likely to have been affected by sewage/manure pollution. This, in principle, fits well with the predominant land use pattern in the area (animal rearing and use of animal manure for farming) observed during the field survey and sampling.

The $\delta^{15}N(NO_3)$ and $\delta^{18}O(NO_3)$ values from borehole #8 (SBA) and hand-dug well #18 (Assamo area), indicate that the high nitrate concentration of those groundwaters could be controlled by the nitrification process (Fig. 5). Taking into account the local oxygen isotope effect during nitrification (Kendall et al., 2007), that is 2/3 of $\delta^{18}O(H_2O)$ between a mean of −1.45% from groundwater and 1/3 from atmospheric oxygen $\delta^{18}O(O_2)$ = +23.88‰ (Barkan and Luz, 2003), a value of approximatively $\delta^{18}O(NO_3)$ = +7‰ is obtained. This latter corresponds to the highest nitrate concentration in hand-dug well #18 (181 mg/l), which could be derived from nitrified manure and/or septic waste. In the other samples investigated, the dual isotope of nitrate shows that the origin could be similar, but the oxygen of nitrate could

612 be due to an increased supply of molecular oxygen (aerial exposure of manure or septic
613 waste?) and/or the effect of a high $\delta^{18}O(H_2O)$ in evaporated rainwater during nitrification
614 (Awaleh et al. 2017a). Indeed, heavily evaporated rainwater up to $\delta^{18}O(H_2O)$ = +5.2 ‰ were
615 collected in the studied region by Fontes et al. (1980). On the other hand, the overall sample
616 trend and a closer look to the inset in Fig. 5 shows that the nitrate concentration and isotope
617 values in the hand dug wells #22, #23, #24 and #32 are controlled by nitrification and
618 denitrification processes being close to the field of the former and paths of the latter (Fig. 5).
619 Apparently, only sample #1 seems to be outside the nitrification and denitrification field and
620 paths, although the lower error bar is not so far from the upper nitrification limit (Fig. 5). In
621 this case, the effect of desert nitrate (saltpeter), as occurred in some samples from the nearby
622 Bara desert area (Awaleh et al. 2017a) and as suggested by Verhagen et al. (1991), should not
623 be excluded. Because of the overlapping isotopic values of reduced nitrogen precursors (Fig.
624 5) and the not ill-defined fractionation effect on oxygen during nitrification (Casciotti et al.,
625 2011), nitrate isotopes can hardly differentiate different sources (Fenech et al., 2012). In other
626 words, the dual isotope approach is not suitable in differentiating closely related sources of
627 nitrate, such as sewage and manure, for the study area (Fig. 5). In addition to the dual isotopes
628 of dissolved nitrate, in some publications the molar ratios of NO_3^-, Cl^-, and K^+ have been used
629 to determine the origin of nitrate (Kovač et al., 2018; Torres-Martínez et al., 2021; Zeng and
630 Wu, 2015). Generally, higher Cl^- concentrations are more characteristic of urban sources,
631 while a higher NO_3^-/K^+ molar ratio was associated with the manure application, and a lower
632 molar ratio is possibly related to urban sewage effluent. However, much of the K and Cl
633 contents of Djibouti waters are attributable to natural water-rock interaction processes. In
634 particular, the high concentration of chloride in the deep waters of the study area, and in the
635 neighboring regions of Dikhil and Arta, is due to the presence of deep-waters of geothermal
636 or marine-geothermal origin. Therefore, the fields and ratios suggested above should be

637 considered with caution in this particular case. While the NO_3^-/K^+ ratio does not seem very
638 useful, the NO_3^-/Cl^- vs Cl^- diagram shows an interesting potential in the studied area (Fig. 6).
639 In this latter plot, the suggested distinction between sewage and manure fields by chloride
640 concentration (Torres-Martínez et al., 2021) seems not to work properly for the studied area
641 (Fig. 6). However, the use of the NO_3^-/Cl^- vs Cl^- variables along with sample dimension
642 proportional to nitrate concentration helps to distinguish samples that exceed WHO nitrate
643 guideline value of 50 mg/l (Fig. 6a). High nitrate samples define a wide ribbon with a slope
644 that departs from fresh Ca-HCO_3/Na-HCO_3 waters towards brackish Na-Cl paleo-waters with
645 increasing chloride concentrations. This ribbon includes the previously suggested manure
646 NO_3^-/Cl^- ratio (Torres-Martínez et al., 2021), while few, if any, low-nitrate freshwater samples
647 are found in the sewage field. Therefore, the major local source of nitrate could be attributed
648 to manure used in local agricultural practices. In particular, it should be noted that the Assamo
649 area has farms that use manure mixed with water as fertilizer (JICA, 2014).
650
651 4.5. Insights from sulfate isotopic composition
652 The isotopic composition of dissolved sulfate, combined with isotopic ratios of other
653 elements, is widely used to define the source of water contamination (Cravotta, 1995; Vitòria
654 et al., 2004). The contribution of sewage and manure to the isotopic composition of dissolved
655 sulfate does not seem to be important. Indeed, none of the samples fell within the typical
656 range of manure and sewage fields (Cravotta, 1995; Otero et al., 2007; Otero et al., 2008;
657 Vitòria et al., 2004) (Fig. 7a). These fields can vary significantly in different regions of the
658 planet. For example, the sulfate isotope values of animal-based organic fertilizers (ABOF)
659 from South Korea have a mean value and standard deviation of $\delta^{34}S(SO_4) = +4.2 \pm 3.7$ ‰ and
660 $\delta^{18}O(SO_4) = +8.4 \pm 6.3$ ‰, i.e., they include both the previously published manure range and
661 the Ali-Sabieh waters (Fig. 7a).

However, applying these isotopic relationships to infer the source of dissolved sulfate should not disregard a careful assessment of natural background contributions (e.g.; Krouse and Mayer, 2000; Cortecci et al., 2008). In this study, the sulfate isotopic composition of groundwater falls within the grid of previously calculated hydrothermal sulfate values (Fig. 7a) (Awaleh et al., 2017b; Awaleh et al., 2020). In particular, the sampled groundwater depicts a main linear trend between two main end-members: (i) ^{34}S–^{18}O enriched groundwater, due to dissolution of gypsum or anhydrite formed at a low hydrothermal temperature ($T \leq 250°C$); (ii) ^{34}S–^{18}O depleted groundwater, due to dissolution of gypsum/anhydrite originating at a high temperature ($T \geq 350°C$). The groundwater with the highest sulfate concentration from Cretaceous sandstone in Ali-Sabieh falls into the latter group (Fig. 7a), which also matches the compositional range of sulfate minerals derived from the oxidation of pyrite or other primary high-temperature hydrothermal sulfides (Moussa et al. 2017). In contrast, most water values from basalt and alluvial deposits are related to the first group, with one sample (#8, Hindi) probably being affected by ^{34}S-enrichment related to bacterial sulfate reduction (Fig. 7a). The contribution of Cretaceous sulfate of marine origin, $\delta^{34}S(SO_4) = +16$ ‰ and $\delta^{18}O(SO_4) = +9$‰ (Turchyn et al., 2009), seems to be negligible in the Ali-Sabieh groundwater borehole. Instead, the sedimentary formation in the Ali-Sabieh area is also characterized by massive amounts of pyrite-rich Jurassic limestone (Gasse, 1986; Varet, 2018). Therefore, it is possible that the presence of gypsum in the upper Cretaceous strata could derive from the oxidation of pre-existing pyrite. This process is common in sandstone formation (e.g., Cortecci et al., 2008), and the newly formed sulfates are called as "terrestrial evaporites", whose depleted isotope composition is not so different from those of hydrothermal origin in Fig. 7a (Clark and Fritz, 1997). Concerning sulfide oxidation, the $\delta^{34}S$ of local pyrite minerals is between +3.6 and +5.3‰ (Moussa et al., 2017), which is quite similar to the ABOF range (Fig. 6a). Therefore, the natural source (pyrite oxidation) could be

misattributed as anthropogenic (organic sources used as fertilizers). However, considering negligible sulfur isotope fractionation during pyrite oxidation (Balci et al., 2007) and a small contribution from more of the ^{34}S-enriched hydrothermal gypsum, the mean values of $\delta^{34}S(SO_4)$ = +6.56 ‰ at Ali-Sabieh could confirm the natural source hypothesis. On the other hand, the $\delta^{18}O(SO_4)$ of these samples depends on the following mass balance during pyrite oxidation (Clark and Fritz, 1997):

$$\delta^{18}O(SO_4) = f_{H2O}\left[\delta^{18}O(H_2O) + \varepsilon^{18}O\left(SO_4\text{-}H_2O\right)\right] + f_{O2}\left[\delta^{18}O\left(O_2\right) + \varepsilon^{18}O(SO_4\text{-}O_2)\right] \quad (4)$$

where $\delta^{18}O(H_2O)$ = -2.75‰ is the mean isotope value of groundwater in Ali-Sabieh; $\delta^{18}O(O_2)$ = +23.88‰ is the isotope composition of molecular atmospheric oxygen (Barkan and Luz, 2003); $\varepsilon^{18}O(SO_4\text{-}H_2O)$ and $\varepsilon^{18}O(SO_4\text{-}O_2)$ are the isotope enrichments that occur during the incorporation of oxygen from water and the incorporation of molecular oxygen into sulfate, respectively; f_{H2O} and f_{O2} = 1- f_{H2O} are the fraction of oxygen from water and atmosphere within the sulfate molecule, respectively. Taking into account the variability of the two enrichment factors ε (Clark and Fritz, 1997; Balci et al., 2007; Heidel et al. 2009), an oxygen fraction of 0.50 ± 0.25 from water and 0.50 ± 0.75 from molecular oxygen in sulfate has been calculated (Fig. 7a). Moreover, considering that nitrate in Ali-Sabieh groundwater is the lowest in the region (~ 3.8 mg/l), the contribution of sulfate from organic compounds such as ABOF could be considered as negligible or nonexistent.

The SO_4/Cl vs. Cl diagram could help to trace the sulfate origin from the different aquifers. The Fig. 6b confirms that the dissolution process of hydrothermal gypsum by meteoric water is the primary source of dissolved sulfate for Na-Cl and Ca-Cl waters (Fig. 7b). It should be noted that the old waters from Ali-Sabieh and the neighboring Dikhil-Arta region both fall on gypsum dissolution curves, without the involvement of seawater (Fig. 7b). For modelling the curves, the React tool of The Geochemist's Workbench® code (Bethke, 2008) was used. It can calculate dissolved ion activities with the B-Dot function, thus providing more reliable

712 data for waters rich in chlorides and sulfates as in this case (Bethke, 2008; Boschetti et al.,
713 2013). For modeling, pure water at 30°C with two different NaCl contents (32 and 64 mmol)
714 was used, and then gypsum was gradually added until saturation. Finally, the fact that the
715 nitrate-rich samples from the Assamo area are on the same mixing line that combines the
716 bicarbonate waters with the Na-Cl waters of Ali-Sabieh, both of which are low in nitrates, is
717 further confirmation of the lack of correlation between the nitrate and sulfate sources.
718 Therefore, it can be concluded that the main source of dissolved sulfate in the studied
719 groundwater is natural and due to water-rock interaction.
720
721 4.6. Origin of CO_2 and ^{14}C-groundwater residence time
722 The calculated $\delta^{13}C(CO_2)g$, obtained by the NetpathXL code from $\delta^{13}C(DIC)$ values and
723 chemical composition, shows a mixing between three potential end-members when compared
724 with the ^{14}C of the studied groundwater samples (Fig. 8). The "modern" end-member (^{14}C =
725 100 pmc) is the CO_2 from soil that, in terms of stable isotope ratio, could be matched with the
726 values range of the local C3-C4 plants, $-21.7‰ < \delta^{13}C(CO_2)g < -21.4‰$ (Adam and Fontes,
727 1984). This substantially agrees with the central values of the broader range proposed more
728 recently and which are valid for the Afar area, $-30.8‰ < \delta^{13}C(CO_2)g < -12.4‰$ (Levin et al.,
729 2004). Groundwater in basaltic aquifers seems to have an important CO_2 contribution from
730 this source, having main values of $^{14}C = 77.4 \pm 8.4$ pmc and $\delta^{13}C(CO_2)g = -18.9 \pm 1.1$ ‰
731 (Fig. 8). Groundwater samples from the Ali-Sabieh sandstone aquifer were significantly less
732 radiogenic (older) but more ^{13}C-enriched, i.e. $^{14}C = 35.4 \pm 4.5$ pmc and $\delta^{13}C(CO_2)g = -11.2 \pm$
733 1.8 ‰, respectively. This agrees with the oxygen and hydrogen stable isotope ratio of the
734 water molecule discussed in section 4.3, from which a more important contribution of paleo-
735 waters in the Ali-Sabieh sandstone aquifer has been hypothesized. This deep paleo-water end-
736 member could have had an important contribution of mantle CO_2, as has also been

737 demonstrated in the waters of the nearby Bara (Dikhil and Arta Provinces; a gray area in Fig.
738 7; Awaleh et al., 2017a), and Hanlé-Gaggadé (Awaleh et al., 2020) aquifer systems. It is
739 interesting to note that in the mid-1980s, isotopic values showed a smaller contribution from
740 paleo-water for the Ali-Sabieh area (Ali-Sabieh 3 in Verhagen et al. 1991 and recalculated in
741 Fig. 8). However, the authors highlighted that the local aquifer was affected by significant
742 exploitation (Verhagen et al. 1991). This suggests that the current increase in older deep water
743 contribution may be attributed to more significant withdrawal from the borehole by residents.
744 Given the different degrees of mixing and the different sources of carbon, it is difficult to
745 estimate the age of all water samples. However, using the different correction models
746 available in the NetpathXL code, it was possible to estimate an age of 6053 ± 1341 years BP
747 for the Ali-Sabieh 1 borehole (ASGA), while for the Galilé borehole (TBA) 431 ± 212 years
748 BP (Table S5, in Supplementary File). In both cases, the values obtained by the different
749 correction models converge, suggesting an interaction with carbonates with A_0 = 65 pm, i.e.
750 formed between the Holocene and the present (Fontes et al., 1980). Due to ion exchange, the
751 mass balance performed by the correction models on Ca and Mg to estimate the contribution
752 of carbonates does not provide reliable values for the samples most affected by this
753 phenomenon. However, for samples with the same lithology as the aquifer, the position in
754 Fig. 8 indicates an age similar to that calculated for the samples discussed above. The age of
755 the Ali-Sabieh groundwater matches with the end of the Holocene East African Humid
756 Period. The main paleo-recharge of these waters is likely due to the additional moisture of
757 that period, which came from the Western Indian Ocean (Liu et al., 2017).
758
759 ## 5. Conclusion
760 The chemical composition of groundwater in the Ali-Sabieh region reveals that most of the
761 samples had a brackish salinity (> 1 g/l) and a predominantly Na-Cl composition. The

762 recharge waters were of Ca-HCO_3 composition, with Na-HCO_3 compositions also found in
763 the literature (JICA, 2014). Compositional evolution can be attributed primarily to water-rock
764 interaction, as is the case for most cold and geothermal waters of similar composition from
765 other parts of the country. Processes such as evaporation and ion exchange contribute to the
766 evolution of the composition, and sometimes generate waters with a peculiar composition
767 (Na-SO_4 and Ca-Cl). Another unusual process in this area is due to the interaction with the
768 sandstone of the Cretaceous formation, which generates waters with high salinity (up to 7 g/l),
769 rich in dissolved sulfates (up to 1,540 mg/l). The stable isotope composition showed that the
770 dissolved sulfate was originated from the oxidation of pre-existing sulfides (possibly within
771 the massive Jurassic limestone). Therefore, the latter terrestrial sulfate is isotopically different
772 from Cretaceous sulfate of marine origin. Despite its natural origin, groundwater in the region
773 is globally classified as “poor” in terms of water quality indices. In addition to salinity, this is
774 mainly due to a high concentration of sulfate (up to 1,540 mg/l) and nitrate (up to 181 mg/l).
775 An evaporitic/desert source of nitrate has been previously invoked (Verhagen et al., 1991) and
776 detected in the desert areas of the nearby Bara (Awaleh et al., 2017a). The presence of paleo-
777 recharged water at Ali-Sabieh related to the Holocene East African Humid Period seems to
778 confirm this hypothesis. Nevertheless, the source of nitrates is to be attributed to increasingly
779 important agricultural practices. In particular, the accumulation of manure in non-waterproof
780 pits near wadis appears to be the most likely cause of the highest nitrate concentration in the
781 Assamo area. This work highlights that current graphs which use chloride and specific
782 characteristic ratios (e.g., Cl/Br, NO_3/Cl) as well as field work to distinguish between
783 different anthropogenic sources are not appropriate for waters at these latitudes. The
784 heterogeneous lithology, the arid climate and the different water-rock interaction processes
785 make the picture very complex. In this case, and in the absence of larger ad-hoc studies in a

similar context, a detailed hydrogeochemical and isotopic study can help distinguish natural and anthropic contributions.

Acknowledgements

This research work was financially supported by the Centre d'Etudes et de Recherche de Djibouti (CERD) and UNESCO through the IGCP 689 project. We would like to thank Pr. Ali Ahmed from the University of Djibouti for proofreading the manuscript. We would like to thank Mr. Osman Youssouf Guedi and Ismael Youssouf Souldan for their assistance in the field work. We would also like to thank Le Conseil Régional d'Ali-Sabieh and La Prefecture d'Ali-Sabieh who provided access to the boreholes and hand dug wells waters in the study area. We would also like to thank three anonymous reviewers for their constructive comments that improved the manuscript.

Table and Figure captions

Table 1. Hydrochemical parameters and isotope data of groundwater samples in the Ali-Sabieh aquifer system

Figure 1. Geological map of the study area (modified from Le Gall et al., 2015). In the inset: a schematic map of the Afar depression and the location of the Republique of Djibouti. The study area is represented by the black rectangle.

Figure 2. Langelier-Ludwig square plot (Langelier and Ludwig 1942; Boschetti 2011), meq/l basis. Open symbols are aquifer-lithology undifferentiated samples from Ali-Sabieh region analyzed by JICA (2014). Light gray area depicts the water composition in the neighbor Bara aquifer system (Dikhil/Arta regions; Awaleh et al. 2017a). Fields with different hatches distinguish meteoric-derived (Abhé; Awaleh et al., 2015a) and seawater-derived (Sakalol,

811 Asal; Awaleh et al., 2017b) geothermal waters, respectively (modified from Awaleh et al.,
812 2017a).
813 **Figure 3.** $\delta^{18}O(H_2O)$ versus $\delta^{2}H(H_2O)$ diagram of the groundwaters from the study area
814 showing the global meteoric water line (GMWL after Craig, 1961) and local meteoric water
815 line (LMWL after Fontes et al., 1979). Gray areas depict the different isotope composition,
816 and probably age, of the aquifers in the neighbor Bara aquifer system (Awaleh et al. 2017a).
817 Error bars on SMOW show the analytical error related to the isotope measurements, i.e.
818 $\delta^{18}O(H_2O) = 0.0 \pm 0.2$ ‰ and $\delta^{18}O(H_2O) = 0.0$ ‰ ± 0.8 ‰. Linear regression show the
819 typical slope related to evaporation in arid climate: S ~ 4.
820 **Figure 4.** Cl/Br (molar ratio) versus Cl concentrations (mg/l) in the studied waters. Symbols
821 as Fig. 2. Gray field depicts the Cl/Br ratio in basalt (Möller et al., 2016); dashed line the
822 seawater ratio in the Gulf of Aden (Awaleh et al. 2015b). Hexagons depict different halides
823 sources according to Alcalá and Custodio (2008): 1 – seawater origin (1b – seawater
824 intrusion); 2 – recharge waters (2a – coastal areas; 2d – coastal arid climate); 3 – leaching of
825 natural evaporites (3a –natural halite; 3b – gypsum containing halite); 4 – volcanic
826 contribution of halides; 5 – Anthropogenic and urban effects (5a – agricultural pollution; 5b –
827 leaching of industrial halite; 5c – leaching of garbage and solid waste; 5d – urban wastewater;
828 5e – septic waste). Ellipses with crosses depict mean and value ranges of septic effluents (SE1
829 - Vengosh and Pankratov, 1998; SE2 - Panno et al., 2006; SE3 – McArthur et al., 2012; SE4 –
830 Rotiroti et al., 2017) and animal manure (AM1 - Panno et al., 2006) from different authors.
831 Mean and standard deviation of Cl/Br ratios in animal manure from Hudak (2003) are also
832 shown by braces and arrows (AM2).
833 **Figure 5.** $\delta^{15}N(NO_3)$ versus $\delta^{18}O(NO_3)$ diagram (a) of the groundwater from the study area, in
834 comparison with nitrates derived from typical: i) N sources after nitrification by local waters

(Aravena and Mayer, 2010; Kendall, 1998; Kendall et al., 2007). Mixed desert nitrates (light gray field), fields and paths modified from Awaleh et al. (2017a).

Figure 6. NO_3/Cl molar ratios versus micro-molar chloride concentration of the groundwater samples from this study and JICA (2014) as bubble-diagram (A), with the sample's areas proportional to NO_3 concentration in mg/l, and as chemical-lithology symbols (B). In (A), on which the samples from this study and JICA (2014) are undistinguished, the dashed line depicts the WHO (2011) nitrate regulation of 50 mg/l. In (B), representative fields of rain, agricultural, soil, sewage and manure inputs adapted from Torres-Martinez et al. (2021). Dotted area enclose groundwater samples with NO_3 > 50 mg/l and depicts the probable mixing with the deeper and high chloride paleo-waters (light gray area shown in both diagrams; dark-gray triangles in B) that were also detected in the Bara desert area (Awaleh et al., 2017a; Verhagen et al., 1991; this study).

Figure 7. Oxygen versus sulfur isotope composition (A) and sulfate/chloride ratio versus sulfate concentration (B), both modified from Awaleh et al. (2017b) and Awaleh et al. (2020). In (A): the grid represents the sulfate composition after disproportionation of local magmatic SO_2 at different temperatures and the H_2S/SO_2 ratio of the deep magmatic gas (Awaleh et al., 2017b). The compositional range of hydrothermal sulfate minerals (Gasse and Fontes, 1989; Moussa et al., 2017) and its trend towards mixed or marine origin is also shown. Lower Cretaceous sulfate isotope from Turchyn et al. (2009). The field of manure (Cravotta, 1997; Otero et al., 2007; Vitòria et al., 2004), sewage (Otero et al., 2008) and animal-based organic fertilizers (ABOF; Shin et al., 2017) are also highlighted. In (B): bricked field represents the compositional range of bicarbonate waters interacting with sedimentary formation and/or from inferoflux aquifer (Awaleh et al. 2017b; Awaleh et al., 2020). Curves depict the interaction of pure water with gypsum at different sality, calculated by React tool of The

Geochemist's Workbench code and thermo.dat dataset (Bethke, 2008). In both diagrams, symbols of the samples as in Fig. 2.

Figure 8. ^{14}C activity (% mc: percent modern carbon) versus the stable isotope ratio $^{13}C/^{12}C$ of the gaseous carbon dioxide, $\delta^{13}C(CO_2)g$. This latter parameter was calculated from the analyzed $\delta^{13}C(DIC)$ and the physico-chemical composition of the groundwater samples via NetpathXL code, version 1.5 (Parkhurst and Charlton 2008). The three light gray fields depict the different groundwater in the Bara aquifer system (Awaleh et al., 2017a; Verhagen et al., 1991) on the base of decreasing ^{14}C-activity: modern (*mod.*), mixed (*mix.*) and old, respectively. The dark gray field was calculated from the samples clustered in the "old" area using the Ca_{solids}-CO_2 isotope-mass balance of the NetpathXL code (Parkhurst and Charlton 2008). The different carbon source fields of soil (Levin et al., 2004), atmosphere (Coplen et al., 2002), and mantle (Awaleh et al., 2017b) are also shown for comparison.

References

Aboubaker, M., 2012. Caractérisation d'un système aquifère volcanique par approche couplée hydrogéochimique et modélisation numérique. Exemple de l'aquifère des basaltes de Dalha, sud-ouest de la République de Djibouti. (PhD thesis). University of Poitiers, France.

Aboubaker M, Jalludin M, Razack M. 2013. Hydrochemistry of a complex volcano-sedimentary aquifer using major ions and environmental isotopes data: Dalha basalts aquifer, southwest of Republic of Djibouti. Environmental Earth Sciences 70**,** 3335-3349. doi.10.1007/s12665-013-2398-8

Adam, A., Fontes, J.C., 1984. Etude Hydrogéologique et hydrochimie de la partie septentrionales de la République de Djibouti. Rapport final pour le Ministèredes Relations Extérieures. Directions des Projets et Développements, contrat n°640-83-941. 170 pp.

Alcalá, F. J., Custodio, E. 2008. Using the Cl/Br ratio as a tracer to identify the origin of salinity in aquifers in Spain and Portugal. Journal of Hydrology, 359(1-2), 189-207. https://doi.org/10.1016/j.jhydrol.2008.06.028

Aravena, R., Mayer, B., 2010. Isotopes and processes in the nitrogen and sulfur cycles. In: Aelion, C.M., Aravena, R., Hunkeler, D., Höhener, P. (Eds.), Environmental Isotopes in Biodegradation and Bioremediation. Chapter 7. CRC Press, pp. 203–246.

Arthaud, F., Jalludin, M. 1993 : Cartographie des fractures d'un réservoir hydrogéologique en milieu volcanique à partir de données HRV de SPOT contrôlées sur le terrain (basaltes miocènes de Djibouti). In: AUPELF-UREF (Ed.), Télédétection et cartographie. Les Presses de l'Université du Québec, pp. 83–94.

Assowe, O.D., Camberlin, P., Pohl, B., Waberi, M.M., Awaleh, M.O., Silah-Eddine, S. 2021. Spatial and temporal variability of rainfall over the Republic of Djibouti from 1946 to 2017. Internaltional Journal of Climatology, 1-20. https://doi.org/10.1002/joc.6986

Assowe, O.D., Awaleh, M.O. Kirk-Davidoff, D., Olauson, J., Söder, L., Awaleh, S.I. 2019. Wind resource assessment and economic analysis for electricity generation in three locations of the Republic of Djibouti. Energy, 185, 884–894. https://doi.org/10.1016/j.energy.2019.07.107.

Audin, L., Quidelleur, X., Coulié, E., Courtillot, V., Gilder, S., Manighetti, I., Kidane, T., 2004. Palaeomagnetism and K-Ar and 40Ar/39Ar ages in the Ali Sabieh area (Republic of Djibouti and Ethiopia): constraints on the mechanism of Aden ridge propagation into southeastern Afar during the last 10 Myr. Geophys. J. Int. 158:327–345.

Awaleh, M.O., Boschetti, T., Adaneh, A.E., Daoud, M.A., Ahmed, M.M., Dabar, O.A., Soubaneh, Y.D., Kawalieh, A.D., Kadieh, I.H., 2020. Hydrochemistry and multi-isotope study of the waters from Hanlé-Gaggadé grabens (Republic of Djibouti, East African Rift System): A low-enthalpy geothermal resource from a transboundary aquifer. Geothermics 2020, 86, 101805. doi.org/10.1016/j.geothermics.2020.101805.

Awaleh, M.O., Boschetti, T., Soubaneh, Y.D., Kim, Y., Baudron, P., Kawalieh, A.D., Ahmed, M.M., Daoud, M.A., Dabar, O.A., Kadieh, I.H., Adiyaman, O., Elmi, S.A., Chirdon, M.A., 2018. Geochemical, multi-isotopic studies and geothermal potential evaluation of the complex Djibouti volcanic aquifer (republic of Djibouti). Applied Geochemistry 97, 301–321. doi.org/10.1016/j.apgeochem.2018.07. 019.

Awaleh, M.O., Baudron, P., Soubaneh, Y.D., Boschetti, T., Hoch, F.B., Egueh, N.M., Jalludi, M., Dabar, O.A., Masse-Dufresne, J, Gassani, J., 2017a. Recharge, groundwater flow pattern and contamination processes in an arid volcanic area: insights from isotopic and geochemical tracers (Bara aquifer system, Republic of Djibouti). Journal of Geochemical Exploration 175, 82-98. doi.org/10.1016/j.gexplo.2017.01.005

Awaleh, M.O., Boschetti, T., Soubaneh, Y.D., Baudron, P., Kawalieh, A.D., Dabar, O.A, Ahmed, M.M., Ahmed, S.I., Daoud, M.A., Egueh, N.M., Mohamed, J. 2017b. Geochemical study of the Sakalol-Harralol geothermal field (Republic of Djibouti): Evidences of a low enthalpy aquifer between Manda-Inakir and Asal rift settings. Journal of Volcanology and Geothermal Research, 331, 26-52. https://doi.org/10.1016/j.jvolgeores.2016.11.008

Awaleh, M.O., Hoch, F.B., Boschetti, T., Soubaneh, Y.D., Egueh, N.M., Elmi, S.A., Jalludin, M., Khaireh, M.A., 2015a. The geothermal resources of the Republic of Djibouti – II: geochemical study of the Lake Abhe geothermal field. J. Geochem. Explor. 159:129–147. http://dx.doi.org/10.1016/j.gexplo.2015.08.011.

Awaleh, M.O., Hoch, F.B., Houssein, K.I., Soubaneh, Y.D., Egueh, N.M., Jalludin, M., Boschetti, T., 2015b. The geothermal resources of the Republic of Djibouti –

I:hydrogeochemistry of the Obock coastal hot springs. Journal of Geochemical Exploration 152, 54–66. doi.org/10.1016/j.gexplo.2015.02.001.

Backer, L.C., Esteban, E., Rubin, C. H., Kieszak, S., McGeehin, M.A., 2001. Assessing acute diarrhea from sulfate in drinking water. Journal-American Water Works Association, 93(9), 76-84. https://doi.org/10.1002/j.1551-8833.2001.tb09288.x

Baird R.B., Eaton A.D., Rice, E.W., 2017. Standard Methods for Examination of Water and Wastewater, 23rd Edition. American Public Health Association (APHA), American Water Works Association (AWWA), Water Environment Federation (WEF), Washington DC, 277 pp.

Balci, N., Shanks III, W.C., Mayer, B., Mandernack, K.W., 2007. Oxygen and sulfur isotope systematics of sulfate produced by bacterial and abiotic oxidation of pyrite. Geochimica et Cosmochimica Acta, 71(15), 3796-3811. https://doi.org/10.1016/j.gca.2007.04.017

Barberi, F., Ferrara, G., Santacroce, R., Varet, J., 1975. Structural evolution of the Afar triplejunction. In: In: Pilger, A., Rösler, A. (Eds.), Afar Depression of Ethiopia 1. Schweizerbart, Stuttgart, Germany, pp. 38–54.

Barberi, F., Varet, J. 1977. Volcanism of Afar: Small-scale plate tectonics implications. Geological Society of America Bulletin, 88, 1251–1266.

Barkan, E., Luz, B., 2003. High-precision measurements of $^{17}O/^{16}O$ and $^{18}O/^{16}O$ of O_2 and O_2/Ar ratio in air. Rapid communications in mass spectrometry, 17(24), 2809-2814. https://doi.org/10.1002/rcm.1267

Batabyal, A. K., Chakraborty, S. (2015). Hydrogeochemistry and water quality index in the assessment of groundwater quality for drinking uses. Water Environment Research, 87(7), 607-617. https://doi.org/10.2175/106143015X14212658613956

Beck, H.E., Zimmermann, N.E., McVicar, T.R., Vergopolan, N., Berg, A., Wood, E.F., 2018. Present and future Köppen-Geiger climate classification maps at 1-km resolution. Scientific Data 5. https://doi.org/10.1038/sdata.2018.214.

Bethke, C.M., 2008. Geochemical and Biogeochemical Reaction Modeling. Second Edition. Cambridge University Press, New York. 543 pp.

Bethke, C.M., Farrel, B., Yeakel, S., 2016. GWB essentials guide. The Geochemist's Workbench® Release 12. Aqueous Solutions, LLC Champaign, Illinois. 186 pp.

BGR (Bundesanstalt für Geowissenschaften und Rohstoffe) 1982. Inventaire et mise en valeur des ressources en eau de la République de Djibouti. Coopération Hydrogéologique Allemande. *Inventory and development of water resources of the Republic of Djibouti*. German Hydrogeological Cooperation. Volume 4.

Boschetti, T., 2011. Application of brine differentiation and Langelier-Ludwig plots to fresh-to-brine waters from sedimentary basins: diagnostic potentials and limits. J. Geochem. Explor. 108:126–130. http://dx.doi.org/10.1016/j.gexplo.2010.12.002

Boschetti, T., De Felice, V., Celico, F., 2013. The Pozzo del Sale groundwaters (Irpinia, Southern Apennines, Italy): origin and mechanisms of salinization. Aquatic geochemistry, 19(4), 303-322. https://doi.org/10.1007/s10498-013-9196-5.

Boschetti, T., González-Hernández, P., Hernández-Díaz, R., Naclerio, G., Celico, F., 2015. Seawater intrusion in the Guanahacabibes Peninsula (Pinar del Rio Province, western Cuba): effects on karst development and water isotope composition. Environmental Earth Sciences, 73(9), 5703-5719. https://doi.org/10.1007/s12665-014-3825-1

Bouh H., 2006. Etude de l'aquifère basaltique de Djibouti et des aquifères adjacents: Approche hydrochimique et isotopique. Thèse de Doctorat, 205p. Université de Paris XI, spécialité Science de la Terre.

Brown RM, McClelland, NI.., Deininger R.A., Tozer R.G. (1970). A water quality index-do we dare? Water Sewage Works 11, 339–343

Brown, R.M., McClelland, N.I., Deininger, R.A., O'Connor, M.F. (1972). A water quality index—crashing the psychological barrier. In: (Thomas, W.A., Ed.) Indicators of environmental quality, pp. 173-182.. Proceedings of a symposium held during the AAAS meeting in Philadelphia, Pennsylvania, December 26–31, 1971. Springer, Boston, MA. https://doi.org/10.1007/978-1-4684-2856-8_15

Caminiti, A.M. 2015. Pierres fines et pierres ornementales en République de Djibouti. Sciences et Environnement, 29, 1–13. ISSN 2409–6245. http://www.scienceetenvironnement.dj

Casciotti, K.L., Buchwald, C., Santoro, A.E., Frame, C., 2011. Assessment of nitrogen and oxygen isotopic fractionation during nitrification and its expression in the marine environment. Methods Enzymol. 486:253–280. https://doi.org/10.1016/B978-0-12-381294-0.00011-0

CCME 2001. CCME Water Quality Index. Technical Report. Canadian Water Quality Guidelinesfor the Protection of Aquatic Life. Canadian Environmental Quality GuidelinesCanadian Council of Ministers of the Environment. Winnipeg - Manitoba.

CCME 2017. Synthesis of research and application of the CCME Water Quality Index. Canadian Council of Ministers of the Environment, Winnipeg - Manitoba.

Chowdhury, A., Adak, M.K., Mukherjee, A., Dhak, P., Khatun, J., Dhak, D. 2019. A critical review on geochemical and geological aspects of fluoride belts, fluorosis and natural materials and other sources for alternatives to fluoride exposure. Journal of Hydrology, 574, 333-359. https://doi.org/10.1016/j.jhydrol.2019.04.033.

Clark, I.D., Fritz, P., 1997. Environmental Isotopes in Hydrogeology. CRC Press, 342 pp.

Coplen, T.B., Hopple, J.A., Boehike, J.K., Peiser, H.S., Rieder, S.E., Krouse, H.R., Rosman, K.J.R., Ding, T., Vocke, R.D.Jr., Révész, K.M., Lamberty, A., Taylor, P., De Bièvre, P., 2002. Compilation of Minimum and Maximum Isotope Ratios of Selected Elements in Naturally Occurring Terrestrial Materials and Reagents. https://pubs.usgs.gov/wri/wri014222/pdf/wri01-4222.pdf

Cortecci, G., Dinelli, E., Boschetti, T., Arbizzani, P., Pompilio, L., Mussi, M., 2008. The Serchio River catchment, northern Tuscany: geochemistry of stream waters and sediments, and isotopic composition of dissolved sulfate. Applied Geochemistry, 23(6), 1513-1543. https://doi.org/10.1016/j.apgeochem.2007.12.031

Craig, H., 1961. Standards for reporting concentrations of deuterium and oxygen-18 in natural waters. Science 133:1702–1703. http://dx.doi.org/10.1126/science.133.3467.1833

Cravotta, C. A. III (1995). Use of stable isotopes of carbon, nitrogen, and sulfur to identify sources of nitrogen in surface waters in the Lower Susquehanna River Basin, Pennsylvania. U.S. Geological Survey (USGS). Open-File Report 94-510. https://doi.org/10.3133/ofr94510

Darling, W.G., 1996. The geochemistry of fluid processes in the eastern branch of the East African Rift System. PhD thesis. British Geological Survey. Open University. https://core.ac.uk/download/pdf/161816903.pdf.

Davies, J. M. (2006). Application and tests of the Canadian water quality index for assessing changes in water quality in lakes and rivers of central North America. Lake and Reservoir Management, 22(4), 308-320. https://doi.org/10.1080/07438140609354365

Edmunds, W.M., Gaye, C.B., 1997. Naturally high nitrate concentrations in groundwaters from the Sahel. J. Environ. Qual. 26:1231–1239. http://dx.doi.org/10.2134/jeq1997.00472425002600050006x.

EPA 2003a. Drinking Water Advisory: Consumer Acceptability Advice and Health Effects Analysison Sulfate. EPA 822-R-03-007. U.S. Environmental Protection Agency, Washington, DC. https://www.epa.gov/sites/production/files/2014-09/documents/support_cc1_sulfate_healtheffects.pdf

EPA 2003b. Contaminant Candidate List Regulatory Determination Support Document for Sulfate. EPA-815-R-03-16. U.S. Environmental Protection Agency, Washington, DC. https://www.epa.gov/sites/production/files/2014-09/documents/support_cc1_sulfate_dwreport.pdf

EPA 2021. National Primary Drinking Water Regulations. U.S. Environmental Protection Agency, Washington, DC. https://www.epa.gov/ground-water-and-drinking-water/national-primary-drinking-water-regulations#Inorganic (last accessed: 2021-06-11)

Fenech, C., Rock, L., Nolan, K., Tobin, J., Morrissey, A., 2012. The potential for a suite of isotope and chemical markers to differentiate sources of nitrate contamination: a review. Water Res. 46:2023–2041. http://dx.doi.org/10.1016/j.watres.2012.01.044.

Fisher, R.S., Mullican III, W.F., 1997. Hydrochemical evolution of sodium-sulfate and sodium-chloride groundwater beneath the northern Chihuahuan Desert, Trans-Pecos, Texas, USA. Hydrogeol. J. 5, 4–16. https://doi.org/10.1007/s100400050102.

Fontes, J.C., Florkowski, T., Pouchan, P., Zuppi, G.M., 1979. Preliminary isotopic study of Lake Asal system (republic of Djibouti). In: Mortimer, C. (Ed.), Application of Nuclear Techniques to the Study of Lake Dynamics, pp. 163–174 (Vienna, Aug. 20–Sept. 2).

Fontes, J.C., Pouchan, P., Saliege, J.F., Zuppi, G.M., 1980. Environmental isotope study of groundwater systems in the Republic of Djibouti. Arid-zone Hydrology: Investigations with Isotope Techniques. IAEA, Vienna, pp. 237–262.

Fontes, J.Ch., Edmunds, W.M., 1989. The Use of Environmental Isotope Techniques in Arid Zone Hydrology - a Critical Review. IHP-III Project 5.2, Document Code: SC/89/ WS/33. Unesco, Paris. https://unesdoc.unesco.org/ark:/48223/pf0000083664

Fritz, P., Fontes, J.C., 1989. Handbook of Environmental Isotope Geochemistry. Elsevier Scientific Pub. Co., New York.

Gadalia, A., 1980. Les Rhyolites du stade initial de l'ouverture d'un rift: Exemple des Rhyolites Miocène de l'Afar. (PhD thesis). University of Orsay, Paris, France.

García, M.G., Borgnino, L., 2015. Fluoride in the Context of the Environment. In: Preedy, V.R. (Ed.), Fluorine: Chemistry. Analysis, Function and Effects: pp. 3–21 http://dx.doi.org/10.1039/9781782628507-00003 (Chapter 1).

Gasse, F., Varet, J., Mazet, G., Recroix, F., Ruegg, J.C., 1986. Carte géologique de la République de Djibouti à 1:100000, Ali Sabieh, notice explicative, ISERST. Ministère français de la Coopération, Paris.

Gasse, F., Fontes, J.C., 1989. Palaeoenvironments and palaeohydrology of a tropical closed lake (Lake Asal, Djibouti) since 10,000 yr B.P. Palaeogeogr. Palaeoclimatol. Palaeoecol. 69:67–102. http://dx.doi.org/10.1016/0031-0182(89)90156-9.

Geiger, R., 1954. Klassifikation der klimate nachW. Köppen. Landolt-Börnstein–Zahlenwerte Und Funkt. Aus Phys. Chem. Astron. Geophys. Und Tech. 3, 603–607.

Gizaw, B., 1996. The origin of high bicarbonate and fluoride concentrations in waters of the Main Ethiopian Rift Valley, East African Rift system. J. Afr. Earth Sci. 22, 391–402. https://doi.org/10.1016/0899-5362(96)00029-2.

Gupta, A.K., Ayoob, S., 2016. Fluoride in Drinking Water: Status, Issues and Solutions. CRC Press, Taylor & Francis Group, Boca Raton, Florida.

Heidel, C., Tichomirowa, M., Junghans, M. 2009. The influence of pyrite grain size on the final oxygen isotope difference between sulphate and water in aerobic pyrite oxidation experiments. Isotopes in environmental and health studies, 45(4), 321-342. https://doi.org/10.1080/10256010903357001

Horton, R.K. 1965. An index number system for rating water quality. Journal of Water Pollution Control Federation, 37(3), 300-306.

Houssein, I., Jalludin, M., 1996. The salinity of Djibouti's aquifer. J. Afr. Earth Sci. 22, 409 – 414. https://doi.org/10.1016/0899-5362(96)00024-3

Huang, T., Pang, Z. 2012. The role of deuterium excess in determining the water salinisation mechanism: A case study of the arid Tarim River Basin, NW China. Applied Geochemistry, 27(12), 2382-2388. https://doi.org/10.1016/j.apgeochem.2012.08.015

Hudak, P.F., 2003. Chloride/bromide ratios in leachate derived from farm-animal waste. Environmental Pollution, 121(1), 23-25. https://doi.org/10.1016/S0269-7491(02)00211-7

ISO, 1998. Water Quality – Determination of Dissolved Li^+, Na^+, NH_4^+, K^+, Mn^{2+}, Ca^{2+}, Mg^{2+}, Sr^{2+} and Ba^{2+} Using Ion Chromatography - Method for Water and Waste Water (ISO 14911:1998). https://www.iso.org/standard/25591.html

ISO, 2007. Water Quality – Determination of Dissolved Anions by Liquid Chromatography of Ions - Part 1: Determination of Bromide, Chloride, Fluoride, Nitrate, Nitrite, Phosphate and Sulfate (ISO 10304–1:2007). https://www.iso.org/standard/46004.html

Jackson, W.A., Böhlke, J.K., Andraski, B.J., Fahlquist, L., Bexfield, L., Eckardt, F.D., Gates, J.B., Davila, A.F., McKay, C.P., Rao, B., Sevanthi, R., Rajagopalan, S., Estrada, N., Sturchio, N.C., Hatzinger, P.B., Anderson, T.A., Orris, G., Betancourt, J., Stonestrom, D., Latorre, C., Li, Y., Harvey, G.J., 2015. Global patterns and environmental controls of perchlorate and nitrate co-occurrence in arid and semi-arid environments. Geochim. Cosmochim. Acta 164:502–522. http://dx.doi.org/10.1016/j.gca.2015.05.016.

Jalludin, M., Razack,M., 2004. Assessment of hydraulic properties of sedimentary and volcanic aquifer systems under arid conditions in the Republic of Djibouti (Horn of Africa). Hydrogeol. J. 12:159–170. http://dx.doi.org/10.1007/s10040-003-0312-2.

Jankowski, J., Acworth, R.I., Shekarforoush, S., 1998. Reverse ion exchange in a deeply weathered porphyritic dacite fracture aquifer system, Yass, New South Wales, Australia. In: G. B. Arehart and J. R. Hulston (Editors), Proceedings of the 9th International Symposium on Water-rock Interaction, Taupo, New Zealand, 30 March - 3 April, 1998, pp. 243 - 246, Balkema, Rotterdam.

JICA 2014. The Master Plan Study Project for Sustainable Irrigation and Farming in Southern Djibouti. Final Report. The Republic of Djibouti. Japan Internation Cooperation Agency (JICA), NTC International Co., Ltd., RD JR 14-104. https://openjicareport.jica.go.jp/833/833/833_404_12183513.html

Kebede, S., 2013. Groundwater in Ethiopia: features, numbers and opportunities. Springer-verlag Berlin Heidelberg. https://doi.org/10.1007/978-3-642-30391-3

Kendall C. 1998. Tracing nitrogen sources and cycling in catchments. In: Kendall, C., McDonnell, J.J. (Eds.), *Isotope Tracers in Catchment Hydrology*. Elsevier Science B.V: Amsterdam; 519-576.

Kendall C., Elliott EM, Wankel SD. 2007. Tracing anthropogenic inputs of nitrogen to ecosystems. In: Michener R.H. and Lajtha K. (eds.), *Stable Isotopes in Ecology and Environmental Science*, 2nd edn., Ch. 12, Oxford Blackwell, 375–449.

Kharaka, Y.K., Hanor, J.S., 2014. Deep fluids in sedimentary basins. In: 2nd ed. In: Holland, H.D., KK, Turekian (Eds.), Treatise on Geochemistry 7. Elsevier, Oxford, pp. 472–515.

Kovač, Z., Nakić, Z., Barešić, J., Parlov, J. 2018. Nitrate origin in the Zagreb aquifer system. Geofluids, 2018.

Krouse, H.R., Mayer, B., 2000. Sulphur and oxygen isotopes in sulphate. In: Cook, P., Herczeg, A.L. (Eds.), Environmental Tracers in Subsurface Hydrology. Kluwer Academic Publishers, pp. 195–231.

Langelier, W.F., Ludwig, H.F., 1942. Graphical methods for indicating the mineral character of natural waters. American Water Works Association Journal 34, 335–352. https://doi.org/10.1002/j.1551-8833.1942.tb19682.x

Le Gall, B., Daoud, M.A., Maury, R.C., Rolet, J., Guillou, H., Sue, C. 2010. Magma-driven antiform structures in the Afar rift: the Ali Sabieh range, Djibouti. J Struct Geol 32:843–854.

Le Gall, B., Daoud AM., Gasse F., Rolet J., Jalludin M., Caminiti AM., Moussa N. 2015: Carte géologique de la République de Djibouti : Echelle 1/200 000. CCGM

Levin, N.E., Quade, J., Simpson, S.W., Semaw, S., Rogers, M., 2004. Isotopic evidence for Plio–Pleistocene environmental change at Gona, Ethiopia. Earth Planet. Sci. Lett. 219 (1-2), 93–110. https://doi.org/10.1016/S0012-821X(03)00707-6.

Liu, X., Rendle-Bühring, R., Kuhlmann, H., Li, A., 2017. Two phases of the Holocene East African Humid Period: Inferred from a high-resolution geochemical record off Tanzania. Earth and Planetary Science Letters, 460, 123-134. https://doi.org/10.1016/j.epsl.2016.12.016.

Manighetti, I., Tapponnier, P., Gillot, P.Y., Jacques, E., Courtillot, V., Armijo, R., Ruegg, J.C., King, G., 1998. Propagation of rifting along the Arabia-Somalia plate boundary: into Afar. J. Geophys. Res. 103:4947–4974. http://dx.doi.org/10.1029/97JB02758.

McArthur, J. M., Sikdar, P. K., Hoque, M., Ghosal, U., 2012. Waste-water impacts on groundwater: Cl/Br ratios and implications for arsenic pollution of groundwater in the Bengal Basin and Red River Basin, Vietnam. Science of the Total Environment, 437, 390-402. https://doi.org/10.1016/j.scitotenv.2012.07.068

McIlvin, M. R., Altabet, M.A., 2005. Chemical conversion of nitrate and nitrite to nitrous oxide for nitrogen and oxygen isotopic analysis in freshwater and seawater. Analytical Chemistry, 77(17), 5589-5595. https://doi.org/10.1021/ac050528s

Mechal, A., Birk, S., Dietzel, M., Leis, A., Winkler, G., Mogessie, A., Kebede, S., 2017. Groundwater flow dynamics in the complex aquifer system of Gidabo River Basin (Ethiopian Rift): a multi-proxy approach. Hydrogeol. J. 25, 519–538. https://doi.org/ 10.1007/s10040-016-1489-5

Meybeck, M. (1987), Global chemical weathering of surficial rocks estimated from river dissolved loads, Am. J. Sci., 287, 401–428. doi:10.2475/ajs.287.5.401.

MAEPH (Ministère de l'Agriculture, de l'Elevage et des Pêches chargé de l'Hydraulique) 2000. Plan d'Action National de Lutte contre la Désertification.

1242 Mlynarski, M., Zlotnicki, J., 2001. Fluid circulation in the active emerged Asal rift (east Africa,
1243 Djibouti) inferred from self-Potential and Telluric – telluric Prospecting. Tectonophysics 339,
1244 455–472. https://doi.org/10.1016/S0040-1951(01)00127-5.
1245
1246 Möller, P., Rosenthal, E., Inbar, N., Magri, F., 2016. Hydrochemical considerations for
1247 identifying water from basaltic aquifers: the Israeli experience. J. Hydrol. 5:33–47.
1248 http://dx.doi.org/10.1016/j.ejrh.2015.11.016.
1249
1250 Moussa, N., Rouxel, O., Grassineau, N.V., Ponzevera, E., Nonnotte, P., Fouquet, Y., Le Gall, B.
1251 2017. Sulfur and strontium isotopic study of epithermal mineralization: a case study from the
1252 SE Afar Rift, Djibouti. Ore Geology Reviews, 81, 358-368.
1253 https://doi.org/10.1016/j.oregeorev.2016.10.028.
1254
1255 Mortimer, M., Müller, J.F., Liess, M., 2014. Sampling Methods in Surface Waters. In: Nollet,
1256 L.M.L., De Gelder, L.S.P. Handbook of Water Analysis. Taylor & Francis Group, Boca
1257 Raton, FL, Chapter 1, pp. 3-46. https://www.routledgehandbooks.com/doi/10.1201/b15314-3
1258
1259 Otero, N., Canals, A., Soler, A., 2007. Using dual-isotope data to trace the origin and processes
1260 of dissolved sulphate: a case study in Calders stream (Llobregat basin, Spain). Aquatic
1261 Geochemistry, 13(2), 109-126. https://doi.org/10.1007/s10498-007-9010-3.
1262
1263 Otero, N., Soler, A., Canals, À., 2008. Controls of $\delta^{34}S$ and $\delta^{18}O$ in dissolved sulphate: learning
1264 from a detailed survey in the Llobregat River (Spain). Applied Geochemistry, 23(5), 1166-
1265 1185. https://doi.org/10.1016/j.apgeochem.2007.11.009
1266
1267 Panno, S.V., Hackley, K.C., Hwang, H.H., Greenberg, S.E., Krapac, I.G., Landsberger, S. and
1268 O'kelly, D.J., 2006. Characterization and identification of Na-Cl sources in ground water.
1269 Groundwater, 44(2), pp.176-187. https://doi.org/10.1111/j.1745-6584.2005.00127.x
1270
1271 Parkhurst, D.L., Appelo C.A.J., 2013. Description of Input and Examples for PHREEQC
1272 Version 3 - A Computer Program for Speciation, Batch-Reaction, One-Dimensional
1273 Transport, and Inverse Geochemical Calculations. U.S. Geological Survey Techniques and
1274 Methods 6-A43, 497 p., https://pubs.usgs.gov/tm/06/a43/.
1275
1276 Parkhurst, D.L., Charlton S.R., 2008. NetpathXL – an Excel Interface to the program
1277 NETPATH. U.S. Geological Survey Techniques and Methods 6-A26, Reston, Virginia.
1278
1279 Pinzutti, P., Humler, E., Manighetti, I., Gaudemer, Y. 2013. Petrological constraints on melt
1280 generation beneath the Asal rift, Djibouti using Quaternary basalts. Geochemistry,
1281 Geophysics, Geosystems, 14, 2932–2953, http://dx.doi: 10.1002/ggge.20187.
1282
1283 Plummer, N., Prestemon, E.C., Parkhurst, D.L., 1994. An interactive code (NETPATH) for
1284 modeling NET geochemical reactions along a flow PATH, version 2.0, U.S. Geological
1285 survey. Water-Resources Investigations Report 94-4169. USGS Earth Science Information
1286 Center, Reston – Virginia. https://doi.org/10.3133/wri944169.
1287
1288 Rock, L., Mayer, B., 2002. Isotopic assessment of sources and processes affecting sulphate and
1289 nitrate in surface water and groundwater of Luxembourg. Isotopes Environm. Health Stud. 38
1290 (4), 191–206.
1291

Rotiroti, M., McArthur, J., Fumagalli, L., Stefania, G. A., Sacchi, E., Bonomi, T., 2017. Pollutant sources in an arsenic-affected multilayer aquifer in the Po Plain of Italy: Implications for drinking-water supply. Science of The Total Environment, 578, 502-512. https://doi.org/10.1016/j.scitotenv.2016.10.215

Schoell, M., Faber, E., 1976. E. Survey on the isotopic composition of waters from NE Africa. Geol. Jahrb. D 17, 197–213.

Schoeller H (1977) Geochemistry of groundwater. In Groundwater studies—An international guide for research and practice. UNESCO, Paris, Ch. 15, pp 1–18).

Shin, W.J., Ryu, J.S., B, M., Lee, K.S., Kim, I. 2017. Nitrogen, Sulfur, and Oxygen Isotope Ratios of Animaland Plant-Based Organic Fertilizers Used in South Korea. Journal of Environmental Quality, 46, 559–567. doi:10.2134/jeq2017.01.0018.

Śliwka-Kaszyńska, M., Kot-Wasik, A., Namieśnik, J. 2003. Preservation and storage of water samples. Critical Reviews in Environmental Science and Technology, 33, 31-44. https://doi.org/10.1080/10643380390814442

Spoelstra, J., Kralt, B. J., Elgood, R. J. 2014. A chemical method for the conversion of nitrate to nitrous oxide for isotopic analysis. National Water Research Institute, Report Number 14-088, Environment Canada.

Stadler, S., Osenbrück, K., Knöller, K., Suckow, A., Sültenfuss, J., Oster, H., Himmelsbach, T., Hötzl, H., 2008. Understanding the origin and fate of nitrate in groundwater of semiarid environments. J. Arid Environ. 72:1830–1842. http://dx.doi.org/10.1016/j.jaridenv.2008.06.003.

Stietljes, L. 1973. L'axe tectono-volcanique d'Asal (Afar central- Territoire français des Afars et des Issas). Thesis, Université de Paris-Sud, Orsay.

Torres-Martínez, J. A., Mora, A., Mahlknecht, J., Daesslé, L. W., Cervantes-Avilés, P. A., & Ledesma-Ruiz, R. 2021. Estimation of nitrate pollution sources and transformations in groundwater of an intensive livestock-agricultural area (Comarca Lagunera), combining major ions, stable isotopes and MixSIAR model. Environmental Pollution, 269, 115445. https://doi.org/10.1016/j.envpol.2020.115445

Turchyn, A.V., Schrag, D.P., Coccioni, R., Montanari, A., 2009. Stable isotope analysis of the Cretaceous sulfur cycle. Earth and Planetary Science Letters, 285(1-2), 115-123. https://doi.org/10.1016/j.epsl.2009.06.002

van Dijk, G., Wolters, J., Fritz, C., de Mars, H., van Duinen, G. J., Ettwig, K. F., Straathof, N., Grootjans, A.P., Smolders, A. J. P. (2019). Effects of groundwater nitrate and sulphate enrichment on groundwater-fed mires: a case study. Water, Air, & Soil Pollution, 230(6), 1-18. https://doi.org/10.1007/s11270-019-4156-3

Varet, J., Gasse, F. 1978. Carte géologique de l'Afar central et méridional ‘Ethiopie et République de Djibouti. CNRS Ed.

Varet, J., 2018. Geology of Afar (East Africa). Regional Geology Reviews. Springer, Cham, Switzerland.

Vengosh A, Pankratov I., 1998. Chloride/bromide and chloride/fluoride ratios of domestic sewage waste-waters and associated contaminated ground water. Ground Water; 36:815–24. https://doi.org/10.1111/j.1745-6584.1998.tb02200.x

Verhagen, B.T., Geyh, M.A., Fröhlich, K., Wirth, K., 1991. Isotope Hydrological Methods for the Quantitative Evaluation of GroundWater Resources in Arid and Semi-arid Areas: Development of a Methodology. Research Reports of the Federal Ministry for Economic Cooperation of the Federal Republic of Germany, Bonn.

Vitòria, L., Otero, N., Soler, A., Canals, À. 2004. Fertilizer characterization: isotopic data (N, S, O, C, and Sr). Environmental science & technology, 38(12), 3254-3262. https://doi.org/10.1021/es0348187.

Walvoord, M.A., Phillips, F.M., Stonestrom, D.A., Evans, R.D., Hartsough, P.C., Newman, B.D., Striegl, R.G., 2003. A reservoir of nitrate beneath desert soils. Science 302: 1021–1024. http://dx.doi.org/10.1126/science.1086435.

WHO 2004. Sulfate in drinking-water. Background document for preparation of WHO Guidelines for drinking-water quality. Geneva, World Health Organization (WHO/SDE/WSH/03.04/114).

WHO 2011. Nitrate and nitrite in drinking-water. Background document for development of WHO Guidelines for Drinking-water Quality. World Health Organization, Geneva, Switzerland.

WHO 2021. Guidelines for drinking water quality, Fourth edition, incorporating the 1st addendum. World Health Organization, Geneva, Switzerland.

Zeng, H., Wu, J. 2015. Tracing the nitrate sources of the Yili River in the Taihu Lake Watershed: A dual isotope approach. Water, 7(1), 188-201. https://doi.org/10.3390/w7010188.

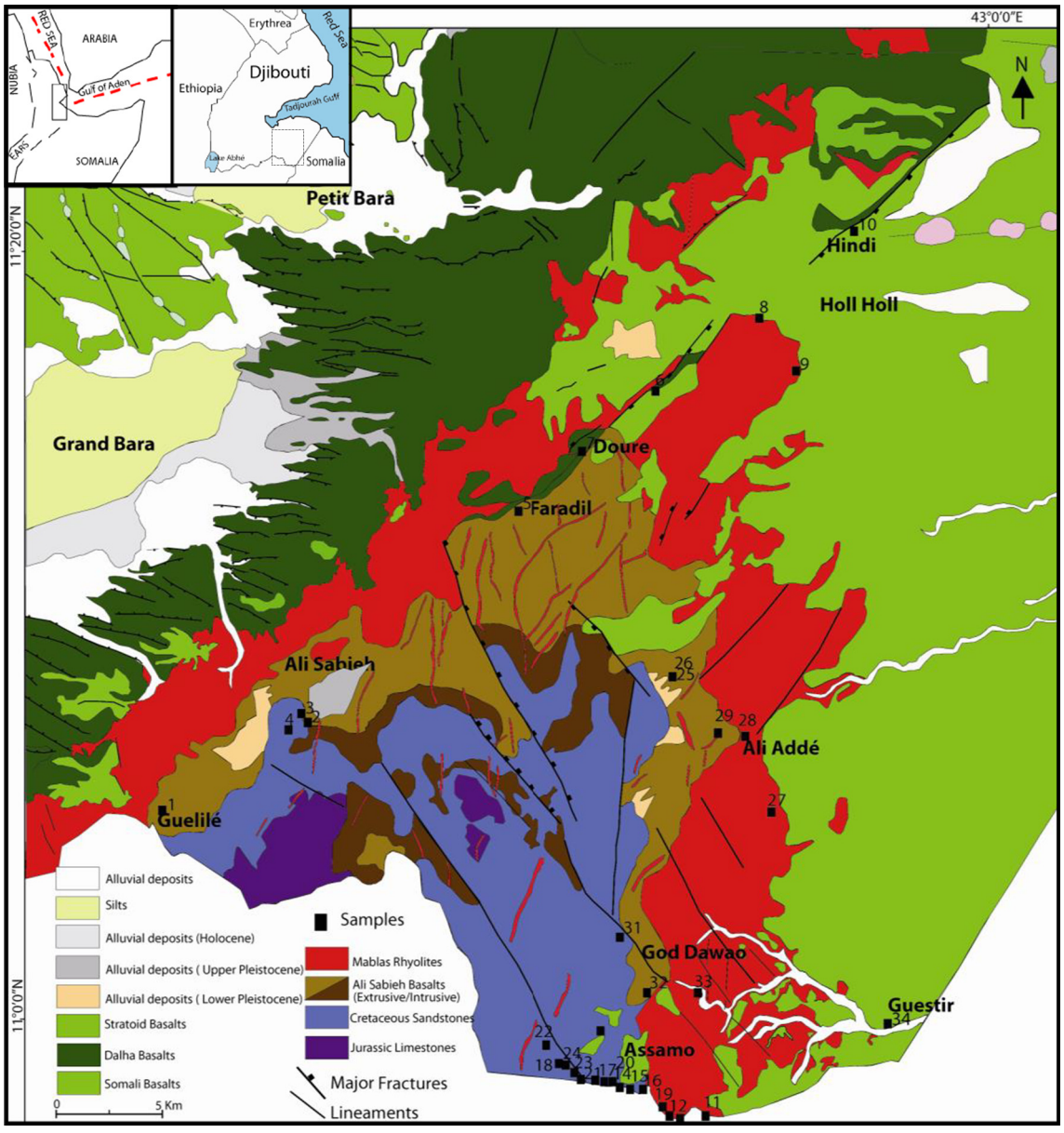
43°0'0"E
11°20'0"N
11°0'0"N
N
Petit Bara
Hindi
Holl Holl
Grand Bara
Doure
Faradil
Ali Sabieh
Ali Addé
Guelilé
God Dawao
Guestir
Assamo
Alluvial deposits
Silts
Alluvial deposits (Holocene)
Alluvial deposits (Upper Pleistocene)
Alluvial deposits (Lower Pleistocene)
Stratoid Basalts
Dalha Basalts
Somali Basalts
Samples
Mablas Rhyolites
Ali Sabieh Basalts (Extrusive/Intrusive)
Cretaceous Sandstones
Jurassic Limestones
Major Fractures
Lineaments
0
5 Km
RED SEA
ARABIA
NUBIA
Gulf of Aden
SOMALIA
EARS
Erythrea
Red Sea
Djibouti
Ethiopia
Tadjourah Gulf
Lake Abhé
Somalia

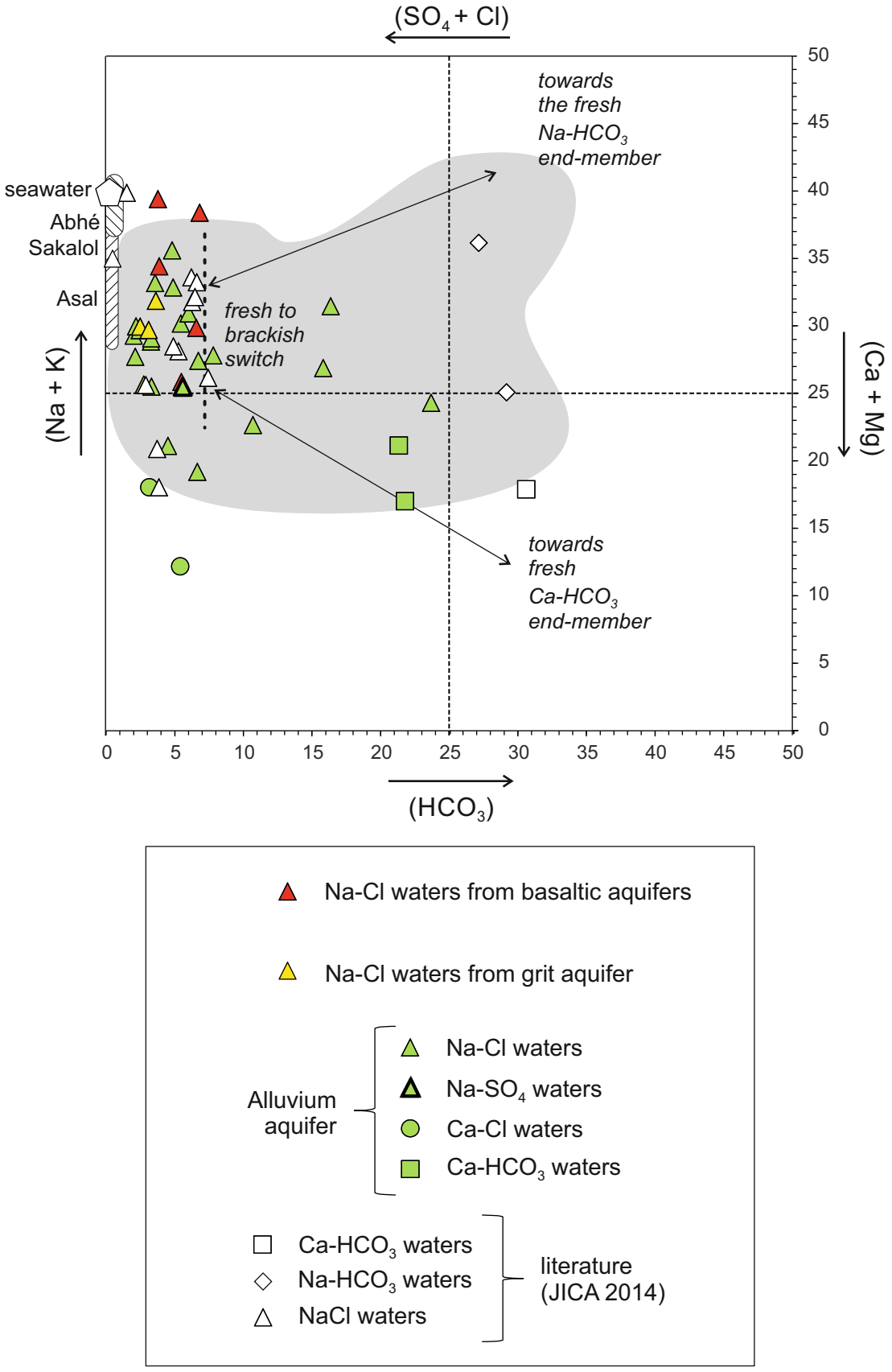
(SO4 + Cl)
towards the fresh Na-HCO3 end-member
seawater
Abhé
Sakalol
Asal
fresh to brackish switch
(Na + K)
(Ca + Mg)
towards fresh Ca-HCO3 end-member
(HCO3)
0
5
10
15
20
25
30
35
40
45
50
Na-Cl waters from basaltic aquifers
Na-Cl waters from grit aquifer
Alluvium aquifer
Na-Cl waters
Na-SO4 waters
Ca-Cl waters
Ca-HCO3 waters
Ca-HCO3 waters
Na-HCO3 waters
NaCl waters
literature (JICA 2014)

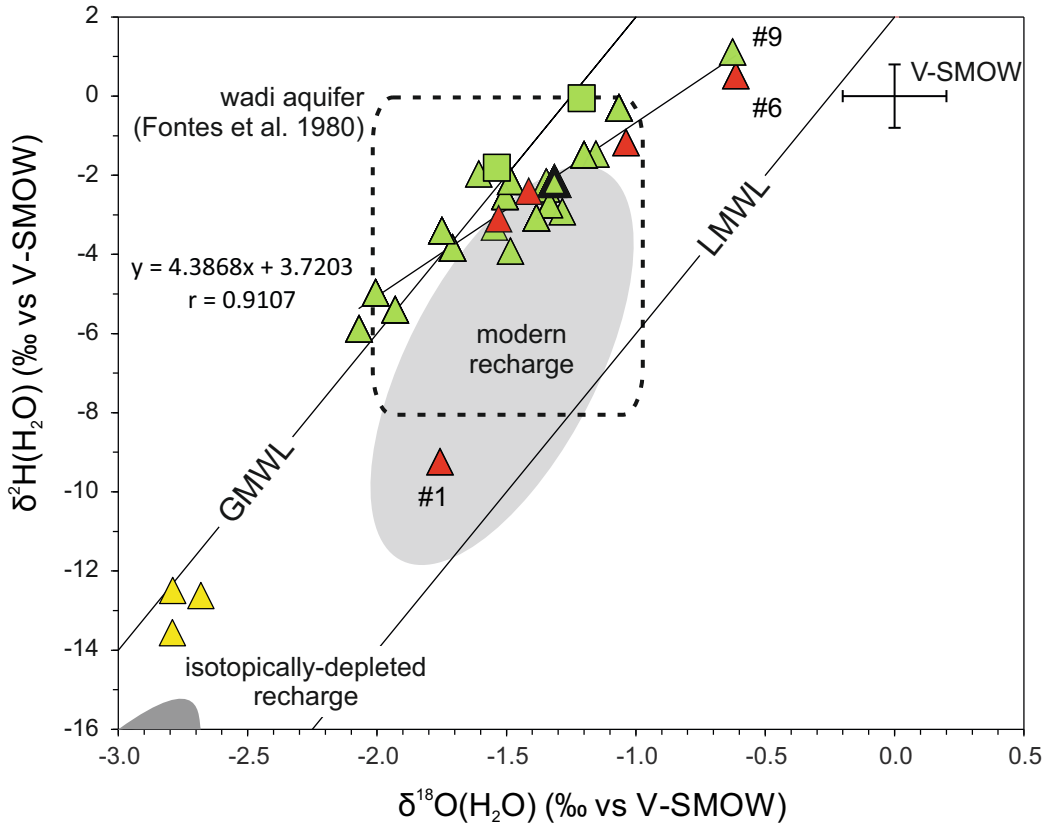
2
0
-2
-4
-6
-8
-10
-12
-14
-16
-3.0
-2.5
-2.0
-1.5
-1.0
-0.5
0.0
0.5
δ²H(H₂O) (‰ vs V-SMOW)
δ¹⁸O(H₂O) (‰ vs V-SMOW)
wadi aquifer
(Fontes et al. 1980)
y = 4.3868x + 3.7203
r = 0.9107
modern
recharge
GMWL
LMWL
#9
#6
#1
V-SMOW
isotopically-depleted
recharge

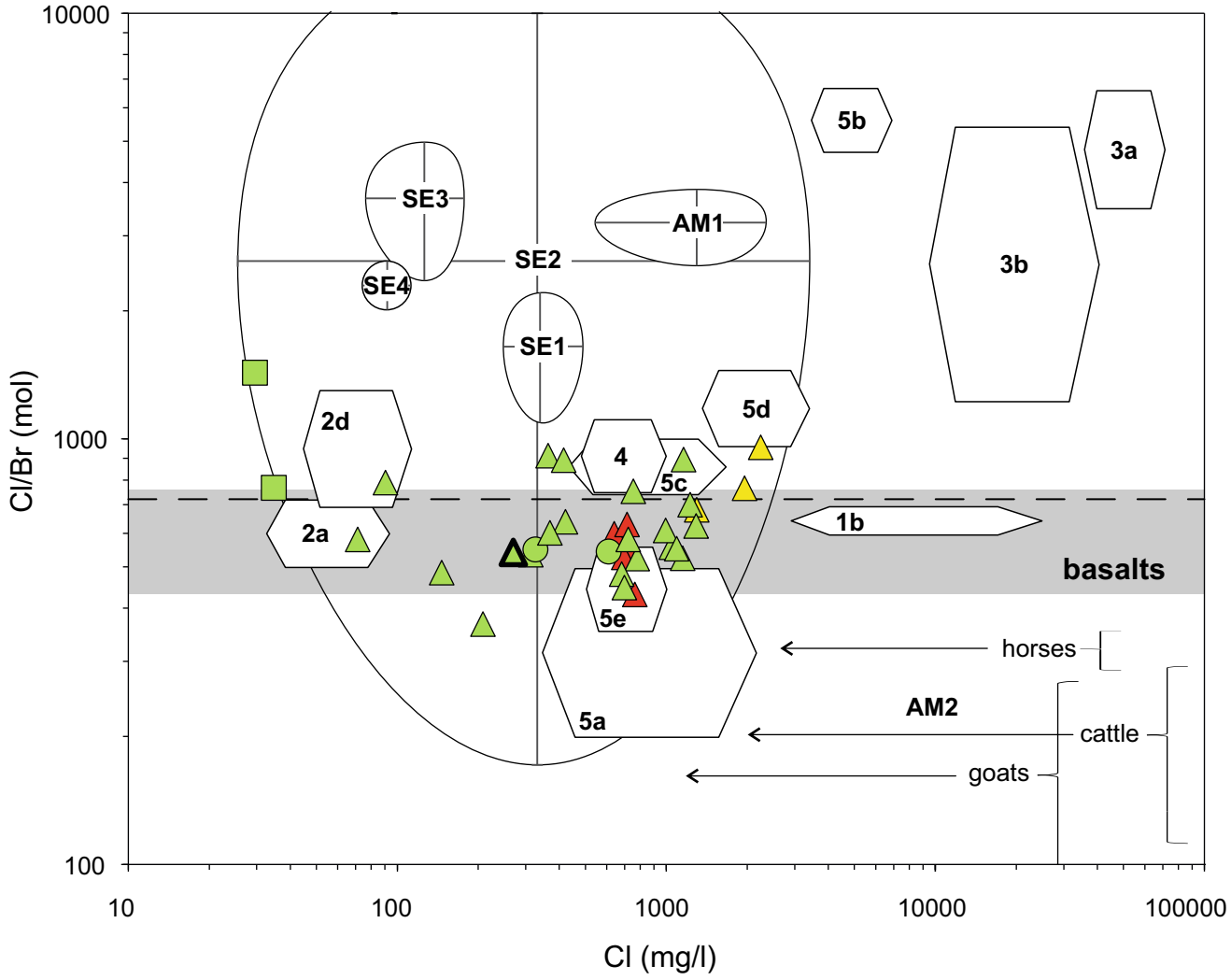
10000
1000
100
Cl/Br (mol)
10
100
1000
10000
100000
Cl (mg/l)
SE3
SE2
SE4
SE1
AM1
5b
3a
3b
2d
5d
4
5c
1b
2a
basalts
5e
5a
horses
AM2
cattle
goats

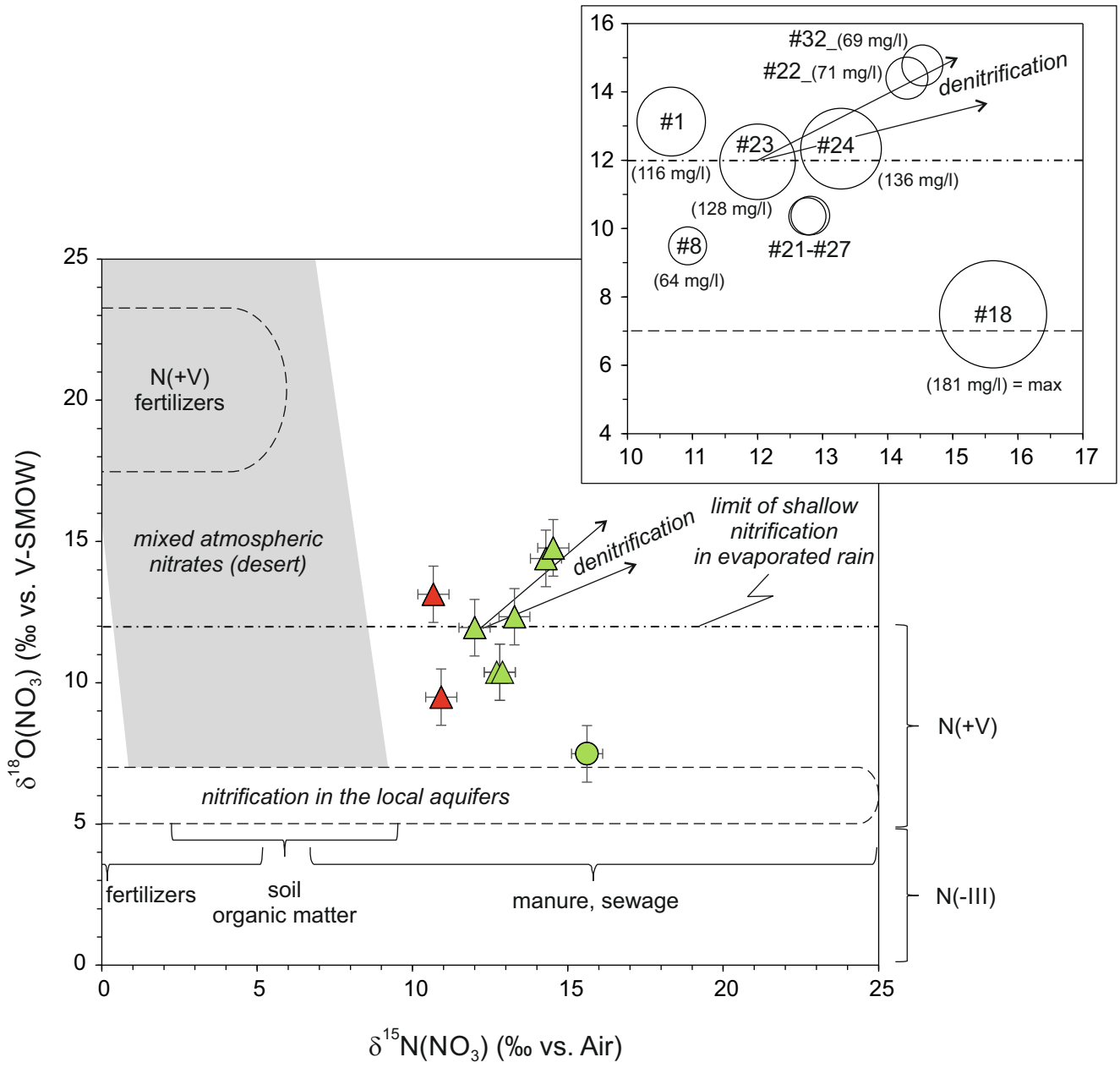
#32_(69 mg/l)
#22_(71 mg/l)
denitrification
#1
#23
#24
(116 mg/l)
(136 mg/l)
(128 mg/l)
#8
#21-#27
(64 mg/l)
#18
(181 mg/l) = max
N(+V)
fertilizers
mixed atmospheric
nitrates (desert)
denitrification
limit of shallow
nitrification
in evaporated rain
nitrification in the local aquifers
N(+V)
N(-III)
fertilizers
soil
organic matter
manure, sewage
δ18O(NO3) (‰ vs. V-SMOW)
δ15N(NO3) (‰ vs. Air)

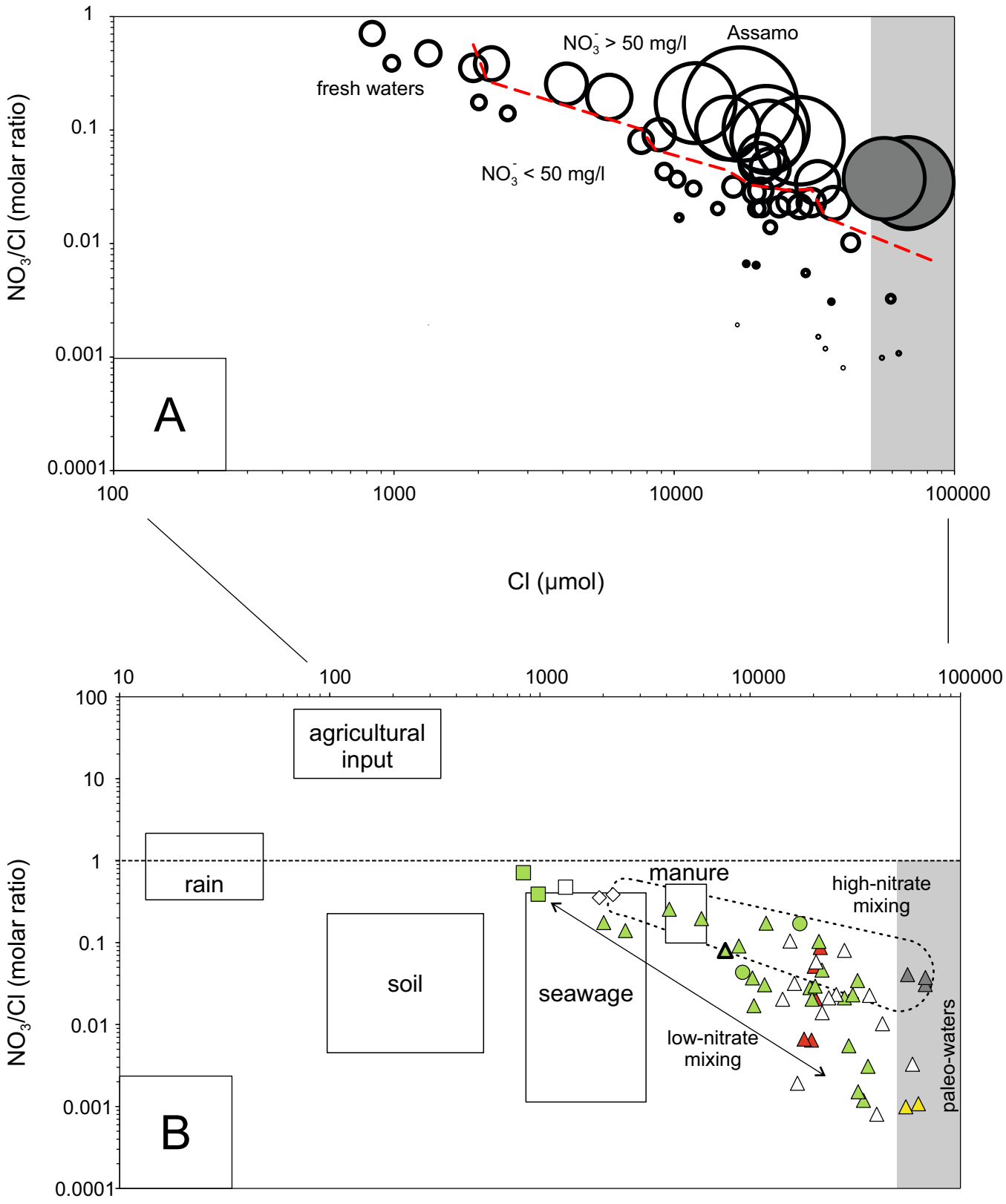
A
fresh waters
NO3- > 50 mg/l
NO3- < 50 mg/l
Assamo
NO3/Cl (molar ratio)
1
0.1
0.01
0.001
0.0001
100
1000
10000
100000
Cl (µmol)
B
agricultural input
rain
soil
seawage
manure
high-nitrate mixing
low-nitrate mixing
paleo-waters
10
100
1000
10000
100000

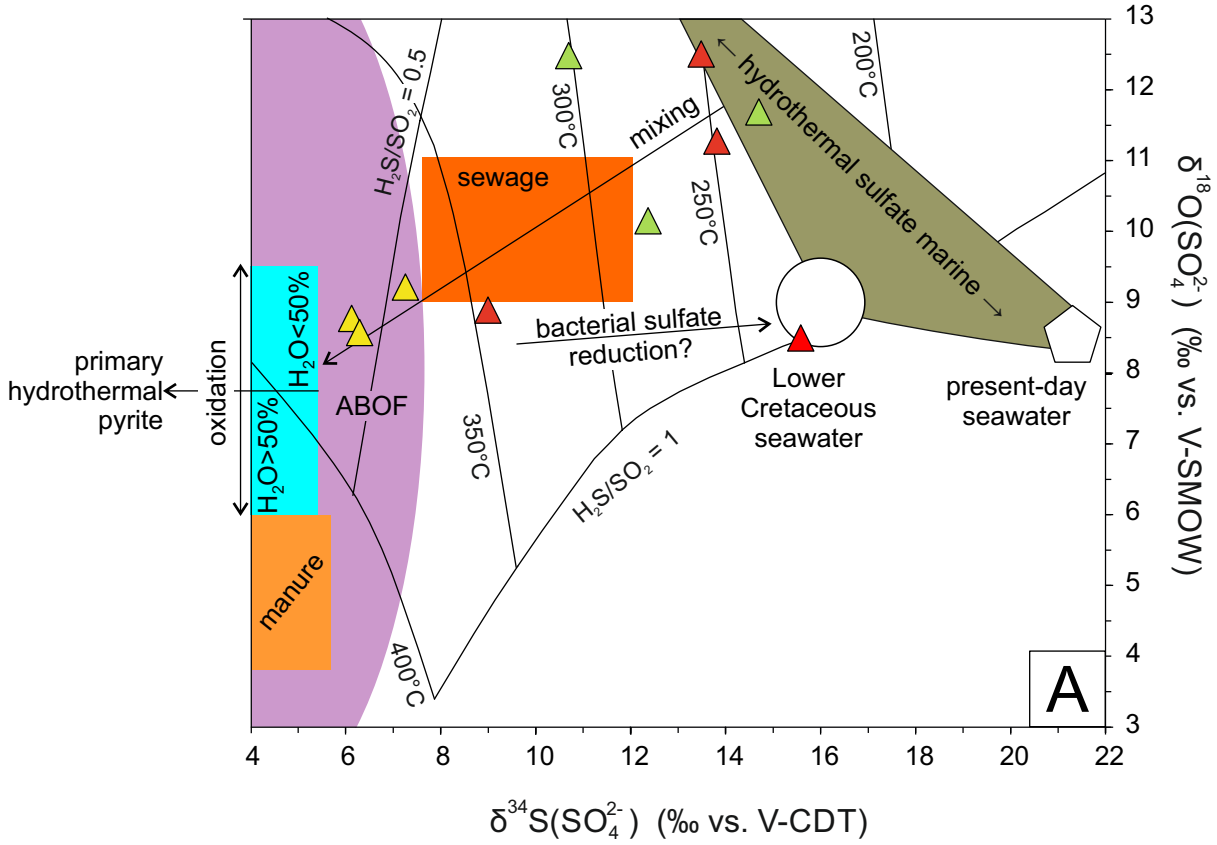
sewage
manure
ABOF
mixing
bacterial sulfate reduction?
hydrothermal sulfate marine
Lower Cretaceous seawater
present-day seawater
primary hydrothermal pyrite
oxidation
H2O<50%
H2O>50%
H2S/SO2 = 0.5
H2S/SO2 = 1
300°C
250°C
200°C
350°C
400°C
A
δ34S(SO4 2-) (‰ vs. V-CDT)
δ18O(SO4 2-) (‰ vs. V-SMOW)

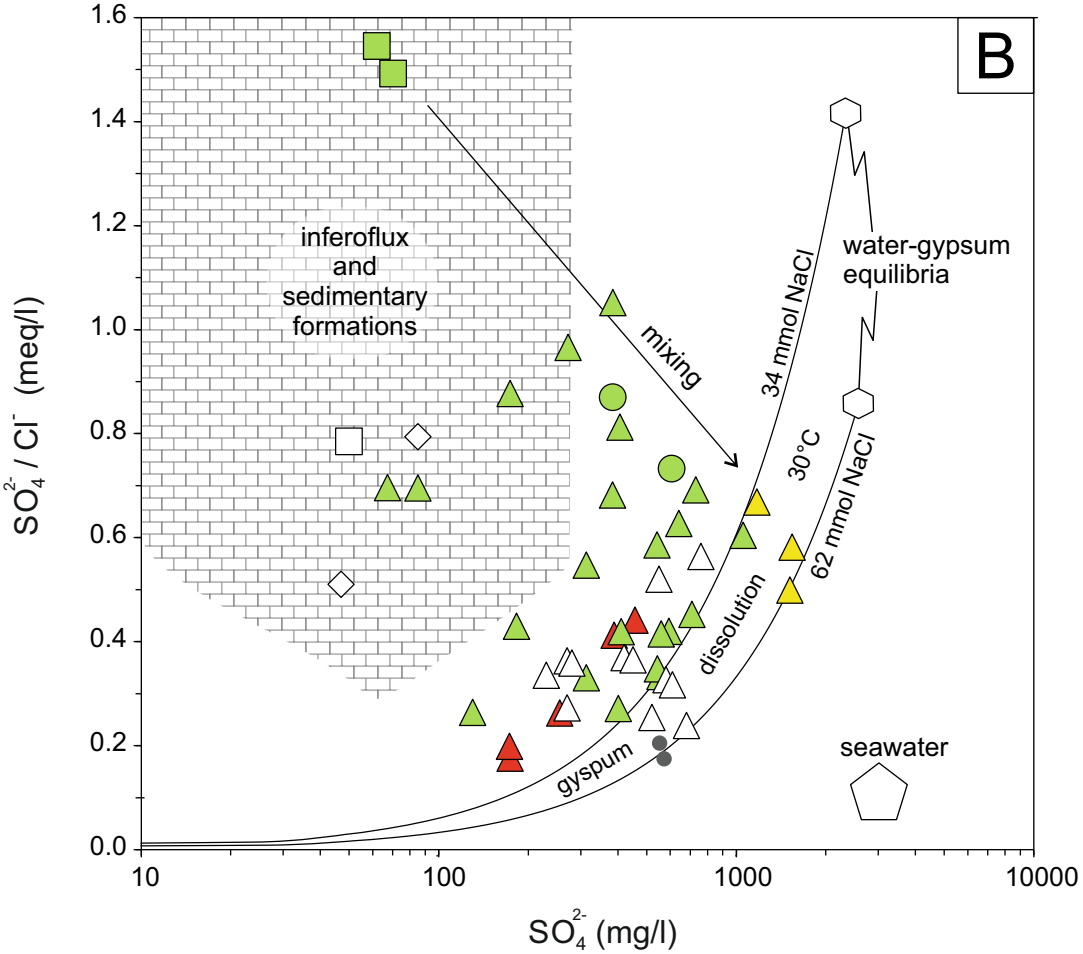
inferoflux and sedimentary formations
mixing
34 mmol NaCl
62 mmol NaCl
30°C
water-gypsum equilibria
dissolution
gyspum
seawater
B
SO4 2- / Cl- (meq/l)
SO4 2- (mg/l)

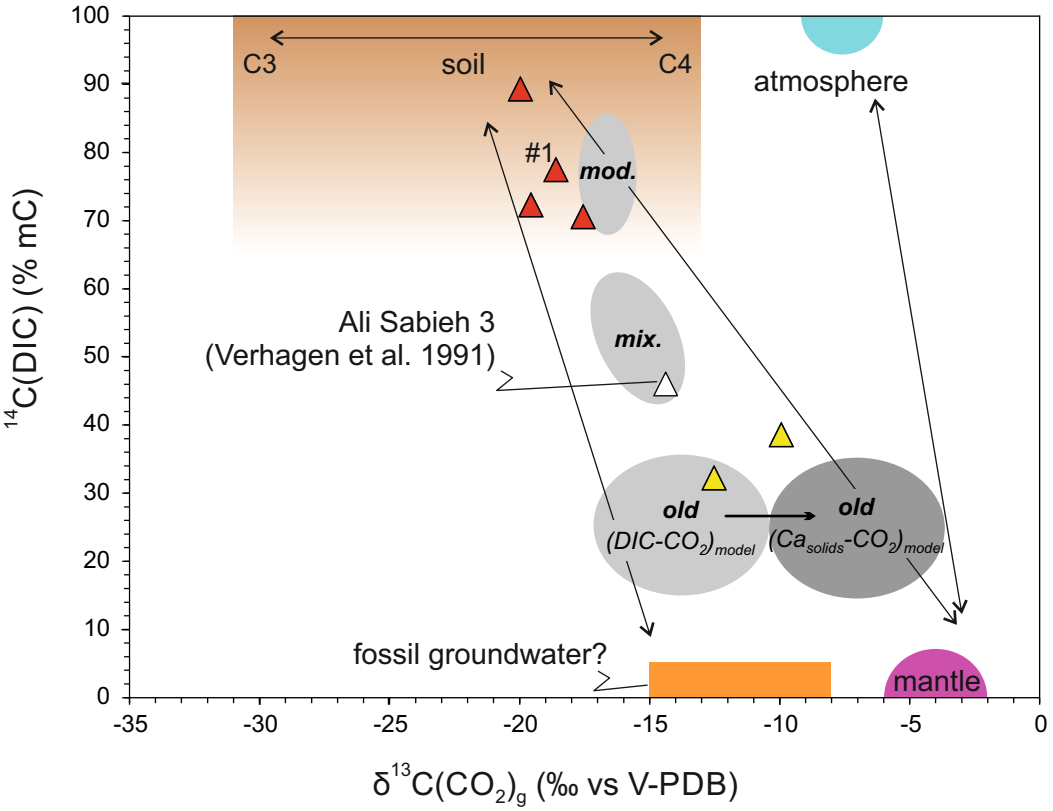
C3
soil
C4
atmosphere
#1
mod.
Ali Sabieh 3
(Verhagen et al. 1991)
mix.
old
(DIC-CO2)model
old
(Casolids-CO2)model
fossil groundwater?
mantle
14C(DIC) (% mC)
δ13C(CO2)g (‰ vs V-PDB)
100
90
80
70
60
50
40
30
20
10
0
-35
-30
-25
-20
-15
-10
-5
0

Table 1. Hydrochemical characteristics (in mg/l) of water samples in the study area

N°	Samples	†TDS		HCO_3	Ca	Mg	Na	K	Cl	SO_4	NO_3	F	Br	IBE	$\delta^{18}O(H_2O)$	$\delta^{2}H\ (H_2O)$	$\delta^{15}N(NO_3)$	$\delta^{18}O(NO_3)$	$\delta^{18}O(SO_4)$	$\delta^{34}S(SO_4)$	$\delta^{13}C(DIC)$	$*\delta^{13}C(CO_2)g$	^{14}C
		(g/l)		(mg/l)	(mg/l)	(mg/l)	(mg/l)	(mg/l)	(mg/l)	(mg/l)	(mg/l)	(mg/l)	(mg/l)	(%)	(‰ vs V-SMOW)	(‰ vs V-SMOW)	(‰ vs AIR)	(‰ vs V-SMOW)	(‰ vs V-SMOW)	(‰ vs V-CDT)	(‰ vs V-PDB)	(‰ vs V-PDB)	(pmc)
1	**Borehole Galilé**	3.0	2976.4	299	128.29	33.51	694.65	1.93	763.82	456.68	116.11	1.40	4.00	2	-1.76	-9.24	10.67	13.1	8.89	9.00	-10.91	-18.6	77.48
2	**Borehole Ali-Sabieh 1**	4.5	4546.6	290	315.50	93.02	938.70	9.67	1295.09	1172.89	-	-	4.28	1	-2.79	-12.49	-	-	8.77	6.13	-3.55	-9.94	38.57
3	**Borehole Ali-Sabieh 2**	6.8	6753.2	300	602.99	141.05	1420.16	19.98	2240.45	1515.75	4.24	1.34	5.28	2	-2.68	-12.62	-	-	8.57	6.29	-5.93	-12.52	32.2
4	**Borehole Ali-Sabieh 3**	6.4	6406.9	350	650.55	98.00	1360.40	7.09	1952.59	1539.50	3.38	0.42	5.75	4	-2.79	-13.56	-	-	9.21	7.26	-	-	-
5	**Borehole Faradil**	1.7	1678.7	120	29.67	51.70	485.28	8.18	726.07	173.49	26.13	2.87	2.95	1	-1.04	-1.17	-	-	11.28	13.82	-10.4	-17.6	70.55
6	**Borehole Dourré**	2.1	2055.3	208	273.08	34.23	397.86	11.14	694.40	388.26	7.84	0.91	2.97	4	-0.61	0.52	-	-	12.51	13.49	-12.23	-20.0	89.28
7	**Borehole Holl-Holl**	1.6	1583.7	200	130.86	52.77	363.54	11.95	640.71	172.83	7.45	0.85	2.41	4	-1.53	-3.1	-	-	-	-	-	-	-
8	**Borehole Hindi**	1.8	1789.8	130	38.95	76.66	413.58	9.53	714.54	254.70	63.99	1.07	2.56	-4	-1.41	-2.40	10.92	9.5	8.50	15.58	-12.01	-19.6	72.31
9	**Hand dug well Dourré**	2.1	2137.8	123	110.80	38.88	388.55	12.35	698.38	313.08	24.86	0.69	3.52	-5	-0.63	1.12	-	-	11.69	14.70	-	-	-
10	**Hand dug well DaaKaay Daloleh**	2.1	2103.0	241	93.99	82.22	419.32	12.54	721.83	410.03	37.21	1.49	2.80	-5	-1.55	-3.31	-	-	-	-	-	-	-
11	**Hand dug well Assamo petit Hijisso 1**	4.2	4238.4	250	438.09	59.32	845.43	14.19	1288.47	1055.06	6.95	1.73	4.65	1	-1.28	-2.92	-	-	-	-	-	-	-
12	**Hand dug well Assamo petit Hijisso 2**	3.0	3023.1	308	183.33	63.42	809.22	13.40	1157.25	709.47	3.06	1.18	2.92	-3	-1.48	-3.92	-	-	-	-	-	-	-
13	**Hand dug well Assamo grand Hijisso**	1.3	1266.7	130	109.74	27.58	336.84	6.92	415.34	383.92	22.17	1.86	1.05	1	-1.15	-1.46			10.15	12.37	-	-	-
14	**Hand dug well Assamo Raregodleh**	0.39	388.9	122	37.18	14.26	79.40	2.68	90.30	85.13	22.14	1.35	0.26	-1	-1.34	-2.35	-	-	-	-	-	-	-
15	**Hand dug well Assamo ancien**	1.2	1205.3	114	157.98	66.75	221.47	5.82	369.19	406.49	10.94	0.57	1.38	5	-	-	-	-	-	-	-	-	-
16	**Hand dug well Gasli-mashe**	1.2	1162.8	120	120.71	39.28	218.26	5.41	270.03	384.88	37.82	1.06	1.13	2	-1.61	-1.96	-	-	-	-	-	-	-
17	**Hand dug well Assamo**	1.2	1230.9	127	256.54	34.44	111.17	8.02	326.42	384.81	24.65	1.93	1.34	2	-	-	-	-	-	-	-	-	-
18	**Hand dug well Assamo 1**	2.3	2268.7	122	352.66	74.04	300.16	12.86	611.32	606.57	181.16	1.02	2.54	3	-1.32	-2.30	15.6	7.5	-	-	-	-	-
19	**Hand dug well Assamo 2**	0.24	237.6	111	52.74	4.36	47.50	4.92	34.80	70.35	23.58	0.25	0.10	5	-1.54	-1.82	-	-	-	-	-	-	-
20	**Hand dug well Assamo 3**	0.29	290.4	100	41.86	10.76	34.21	1.86	29.62	62.00	36.82	2.71	0.05	2	-1.21	-0.06	-	-	-	-	-	-	-
21	**Hand dug well Assamo 4**	0.77	765.8	230	55.26	28.45	196.29	4.30	146.24	173.81	65.26	2.23	0.68	4	-1.51	-2.53	12.9	14.6	-	-	-	-	-
22	**Hand dug well Assamo 5**	0.92	924.1	109	84.60	26.90	176.04	5.98	207.84	272.04	71.09	0.86	1.28	1	-1.48	-2.15	14.3	14.4	-	-	-	-	-
23	**Hand dug well Assamo 6**	1.4	1437.7	172	133.27	92.70	202.39	3.32	422.20	312.92	127.56	1.51	1.49	0	-1.33	-2.74	12.0	12.0	-	-	-	-	-
24	**Hand dug well Assamo 7**	2.5	2495.8	258	107.39	135.29	576.37	2.23	753.97	641.00	136.07	2.10	2.26	1	-1.71	-3.83	13.3	12.3	-	-	-	-	-
25	**Hand dug well Ali-Addé 1**	3.1	3073.1	125	138.17	160.27	564.47	16.19	1226.58	553.34	2.55	1.25	3.95	-3	-1.07	-0.30	-	-	-	-	-	-	-
26	**Hand dug well Ali-Addé 2**	3.2	3157.0	180	154.57	176.67	524.37	13.59	1043.48	594.00	10.06	1.00	4.23	0	-1.20	-1.48	-	-	12.48	10.69	-	-	-
27	**Hand dug well Ali-Addé 3**	2.3	2341.2	95	236.11	48.31	506.42	9.33	778.89	730.54	62.78	1.21	3.35	-2	-1.07	-0.30	12.8	10.4	-	-	-	-	-
28	**Hand dug well Ali-Addé 4**	2.1	2068.1	108	256.03	46.81	398.67	7.47	683.00	542.12	33.72	1.10	3.20	2	-1.38	-3.08	-	-	-	-	-	-	-
29	**Hand dug well Dannan Ali-Addé**	2.4	2420.3	110	124.25	145.43	616.61	14.93	994.85	559.40	36.77	1.66	3.68	4	-1.93	-5.40	-	-	-	-	-	-	-
30	**Hand dug well God-dawao 1**	0.85	846.8	146	89.01	30.55	198.46	3.57	363.14	129.90	23.46	1.70	0.90	0	-2.07	-5.88	-	-	-	-	-	-	-
31	**Hand dug well God-dawao 2**	0.44	438.5	187	50.90	15.67	79.30	6.75	71.22	67.19	21.82	1.39	0.28	4	-2.01	-4.96	-	-	-	-	-	-	-
32	**Hand dug well Dousseyeh**	3.1	3118.2	186	107.86	167.44	593.50	12.81	1150.35	542.61	69.23	1.62	4.95	-3	-1.23	-2.60	14.5	14.8	-	-	-	-	-
33	**Hand dug well Bio-Khalaf**	0.98	977.9	210	115.50	33.82	157.90	8.38	313.26	182.47	49.87	1.34	1.32	-4	-1.75	-3.40	-	-	-	-	-	-	-
34	**Hand dug well Guestir**	2.7	2672.9	123	76.58	170.38	592.25	12.02	1092.19	401.64	43.86	1.83	4.46	2	-1.35	-2.18	-	-	-	-	-	-	-

† mean between measured (Table S2) and calculated TDS values, the latter according to Baird et al. (2017): TDS (g/l) = (HCO_3 x 0.5) + Ca + Mg + Na + K + Cl + SO_4 + NO_3 + F + Br;

\- not detected or not measured;

IBE Ionic Balance Error;

* values calculated by NetpathXL code (gas-solution equilibrium).